DEVELOPMENT OF A TSUNAMI FORECAST MODEL FOR Nikolski, Alaska (DRAFT)

Yong Wei

June, 2012

Abstract

As part of NOAA's tsunami forecast system, this study addresses the development, validation, and stability tests of the tsunami forecast model for Nikolski, Alaska. Based on the Method of Splitting Tsunami (MOST), two tsunami forecast models were constructed in the present study. Using same B and C grid, with a spatial resolution of 2 arc sec (x axis) and 1 arc sec (y axis) in C grid, the two models (forecast model 1 and forecast model 2) provide different coverage of the tsunami wave propagation in A grid. Forecast model 1 employs an A grid with small coverage and slightly coarser grid resolution, and it can accomplish a 4-hour simulation of wave inundation onto dry land within 12 minutes of CPU time. Forecast model 2 covers larger area in A grid to provide more accurate computation of tsunami wave dynamics over shallow continental shelf, but requires more computational time. In parallel, a reference inundation model is developed using grids of higher resolution to provide model references for both forecast models. The Nikolski forecast models were carefully evaluated using three historical tsunami events. The model validations show good agreement between model results and observations at the Nikolski tide station. The modeling results obtained using forecast model 2 and the reference model are highly consistent. The stability of all models is further evaluated based on 21 synthetic scenarios generated in the major subduction zones in the Pacific Rim at magnitudes of M_w 9.3, M_w 7.5 and M_w 6.4.

1. Background and Objectives

The National Oceanic and Atmospheric Administration (NOAA) Center for Tsunami, Research (NCTR) at the NOAA Pacific Marine Environmental Laboratory (PMEL) has developed a tsunami forecasting capability for operational use by NOAA's two Tsunami Warning Centers located in Hawaii and Alaska (Titov *et al.*, 2005a). The system is designed to efficiently provide basin-wide warning of approaching tsunami waves accurately and quickly. The system, termed Short-term Inundation Forecast of Tsunamis (SIFT), combines real-time tsunami event data with numerical models to produce estimates of tsunami wave arrival times and amplitudes at a coastal community of interest. The SIFT system integrates several key components: deep-ocean observations of tsunamis in real time, a basin-wide pre-computed propagation database of water level and flow velocities based on potential seismic unit sources, an inversion algorithm to refine the tsunami source based on deep-ocean observations during an event, and high-resolution tsunami forecast models.

The objective of this present work is to develop an operational forecast model to be used in near real time to protect the community of Nikolski, Alaska, from the potential impact

posed by a tsunami. Nikolski, Alaska is a small coastal community located off the southwest end of Umnak Island, one of the Fox Islands. According to Census 2010, the total population in Nikolski is 18 (http://censusviewer.com/city/AK/Nikolski), a drop of 21 from 39 in Census 2000. In 2010, there were 23 housing units in the community and 13 were occupied. Nikolski is one of the oldest continuously-occupied community in the world, dating as far back as 8,5000 years ago. However, the drop of population has resulted serious social impact to the community – the school was shutdown due to lack of attendees, which forced the redsients, especially the younger generation, to leave Nikolski. The village of Nikolski is located in a biologically prime, diverse, and productive area, a fact that has contributed to the continuous habitation of the general area for at least 8,500 years. Most of the neighboring islands are in the Aleutian National Wildlife Refuge. Nikolski is adjacent to the rich fisheries area of the Bering Sea and Alaska/Aleutian shelf and within a prime king crab area. Although there are no mineral deposits in Umnak Island, the general area in the Bering Sea are known for potential outer continental shelf oil and gas fields. Subsistence activities, sheep and cattle raising, and fishing-related employment sustain the community.

Historically, Nikolski is a coastline impacted from tsunami infrequently. However, the costal community did suffer from up to 12 m tsunami runup and large tsunami inundation during the 1946 Alaska tsunami (Landers, 1999). The vulnerability of tsunami hazards at Nikolski has never been thoroughly evaluated and studied. The development of Nikolski tsunami forecast model provides a valuable modeling tool to the efforts of tsunami hazard assessment in Nikolski, and more importantly another essential contribution to the existing NOAA's tsunami forecasting system in the Pacific.

2. Forecast Methodology

A high-resolution inundation model was used as the basis for development of a tsunami forecast model to operationally provide an estimate of wave arrival time, wave height, and inundation at Nikolski, Alaska following tsunami generation. All tsunami forecast models are run in real time while a tsunami is propagating across the open ocean. The Nikolski model was designed and tested to perform under stringent time constraints given that time is generally the single limiting factor in saving lives and property. The goal of this work is to maximize the length of time that the community of Nikolski has to react to a tsunami threat by providing accurate information quickly to emergency managers and other officials responsible for the community and infrastructure.

The general tsunami forecast model, based on the Method of Splitting Tsunami (MOST), is used in the tsunami inundation and forecasting system to provide real-time tsunami forecasts at selected coastal communities. The model runs in minutes while employing high-resolution grids constructed by the National Geophysical Data Center. MOST is a suite of numerical simulation codes capable of simulating three processes of tsunami evolution: earthquake, transoceanic propagation, and inundation of dry land. The MOST model has been extensively tested against a number of laboratory experiments and benchmarks (Synolakis *et al.*, 2008) and was successfully used for simulations of many historical tsunami events. The main objective of a forecast model is to provide an accurate, yet rapid, estimate of wave arrival time, wave height, and inundation in the

minutes following a tsunami event. Titov and González (1997) describe the technical aspects of forecast model development, stability, testing, and robustness, and Tang *et al*. (2009) provide detailed forecast methodology.

A basin-wide database of pre-computed water elevations and flow velocities for unit sources covering worldwide subduction zones has been generated to expedite forecasts (Gica *et al.*, 2008). As the tsunami wave propagates across the ocean and successively reaches tsunameter observation sites, recorded sea level is ingested into the tsunami forecast application in near real-time and incorporated into an inversion algorithm to produce an improved estimate of the tsunami source. A linear combination of the pre-computed database is then performed based on this tsunami source, now reflecting the transfer of energy to the fluid body, to produce synthetic boundary conditions of water elevation and flow velocities to initiate the forecast model computation.

Accurate forecasting of the tsunami impact on a coastal community largely relies on the accuracies of bathymetry and topography and the numerical computation. The high spatial and temporal grid resolution necessary for modeling accuracy poses a challenge in the run-time requirement for real-time forecasts. Each forecast model consists of three telescoped grids with increasing spatial resolution in the finest grid, and temporal resolution for simulation of wave inundation onto dry land. The forecast model utilizes the most recent bathymetry and topography available to reproduce the correct wave dynamics during the inundation computation. Forecast models, including the NIkolski model, are constructed for at-risk populous coastal communities in the Pacific and Atlantic Oceans. Previous and present development of forecast models in the Pacific (Titov *et al*., 2005; Titov, 2009; Tang *et al*., 2008; Wei *et al*., 2008; Tang *et al*., 2012; Wei *et al.*, 2012) have validated the accuracy and efficiency of each forecast model currently implemented in the real-time tsunami forecast system. Models are tested when the opportunity arises and are used for scientific research. Tang *et al*. (2009) provide forecast methodology details.

3. Model development

The general methodology for modeling at-risk coastal communities is to develop a set of three nested grids, referred to as A, B, and C-grids, each of which becomes successively finer in resolution as they telescope into the population and economic center of the community of interest. The offshore area is covered by the largest and lowest resolution A-grid while the near-shore details are resolved within the finest scale C-grid to the point that tide gauge observations recorded during historical tsunamis are resolved within expected accuracy limits. The procedure is to begin development with large spatial extent merged bathymetric topographic grids at high resolution, and then optimize these grids by sub sampling to coarsen the resolution and shrink the overall grid dimensions to achieve a 4 to 10 hr simulation of modeled tsunami waves within the required time period of 10 min of wall-clock time. The basis for these grids is a high-resolution digital elevation model constructed by the National Geophysical Data Center and NCTR using all available bathymetric, topographic, and shoreline data to reproduce the wave dynamics during the inundation computation for an at-risk community. For each community, data are compiled from a variety of sources to produce a digital elevation model referenced to Mean High Water in the vertical and to the World Geodetic System

1984 in the horizontal (http://ngdc.noaa.gov/mgg/inundation/tsunami/inundation.html). From these digital elevation models, a set of three high-resolution, "reference" elevation grids are constructed for development of a high-resolution reference model from which an 'optimized' model is constructed to run in an operationally specified period of time. The operationally developed model is referred to as the optimized tsunami forecast model or forecast model for brevity.

3.1 Forecast area

Southern Umnak Island contains the glaciated volcanic mountains in the northern part and the Nikolski plain the southern part. The Nikolski plain is a rolling surface about 100 m in average altitude. Except for a few scattered patches of questionable till and some flanking beach deposits, the Nikolski plain is free of surficial deposits, but its surface is dotted with many undrained depressions, some of which serve as basins for small lakes less than a 2 km long. A few of the lakes near the coast have been drained by the cutting down of their outlets, and all of these former outlets are now youthful V-shaped gorges. The majority of the lakes have not been altered since they were formed (Byers, 1959). Byers (1959) suggested that the Nikolski plain is an uplifted portion of the shelf somewhat modified by extensive piedmont glaciation. Nikolski has a mean annual temperature of 4 °C and a mean annual precipitation of 785 mm.

The NOS Nikolski tide station is housed 700 m northwest to Nikolski residential area (**Figure 1**). The water depth at the gage sensor is 2.36 m (water level difference between the Mean High Water and the Chart Datum). This National Ocean Service (NOS) station was established on 28 June 2006. The local mean tide range is about 0.84 m, and the diurnal range is 1.23 m.

3.2 Historical events and data

National Geophysical Data Center (NGDC)'s tsunami runup database (http://www.ngdc.noaa.gov/hazard/tsu.shtml) shows that there have been a few historical tsunamis affecting the coastline of Nikolski (**Figure 2** and **Table 1**).

Lander (1996) reported that Nikolski Bay ran dry in the 1940's (probably 1946). The wave was reported over the bank and near the road; driftwood was washed up on the ice of a lake a quarter of a mile from the Bering Sea coast. It was not clear what the runup height is in Nikolski Bay. Lander (1996) reported a 12-m wave runup on the Pacific coast side of Umnak Island, and the beach there also showed signs of erosion. The 1946 tsunami is probably the only event in recorded history that had brought inundation to Nikolski coastline. After NOS station was established in Nikolski on 28 June 2006, three small tsunamis, all generated by distant earthquakes, were documented for Nikolski community between 2006 and 2009. The time series at the tide station indicates that the 15 November 2006 Kuril tsunami generated a maximum of 19 cm wave amplitude, while the other two (29 September 2009 Samoa and 7 October 2009 Vanuatu) only brought waves smaller than 10 cm. The 11 March 2011 Japan tsunami, generated by an Mw 9.0 earthquake 4,000 km away, produced 84 cm tsunami amplitude at Nikolski tide station. No tsunami inundation was reported along Nikolski coastline. The 24 June 2011 Fox Islands Mw 7.2 earthquake occurred only 220 km southwest of Nikolski, and generated a

small tsunami that was recorded by tide stations as far as Hilo, Hawaii (6 cm) and Midway (4 cm). Nikolski station reported the largest tsunami amplitude, 10 cm, of this event.

3.3 Model setup

3.3.1 Grid boundary and resolution

The continental shelf along Aleutian Islands complicates the modeling of tsunami waves approaching the shoreline there. When a tsunami reaches continental shelf and begins to shoal, it will slow down and increase in height while introducing model diffusion and dispersion. Burwell et al. (2007) studied the diffusion and dispersion characterization of MOST model, and concluded that the nature of the scheme, at all resolvable wave numbers, is diffusive and dispersive for $\beta = (gd)^{1/2}\Delta t/\Delta x \neq 1$, where Δt is the temporal step and Δx is the space step. Diffusive effects are stronger for poorly resolved waves (large space step compared to wave length). As β decreases, diffusive effects are reduced and dispersion continues to increase. Thus, numerical dispersion can be an issue closer to shore, but can be controlled through a careful choice of β, or in other words, the ratio between Δt and Δx. The tsunami propagation database (Gica et al., 2008) was developed at a grid spacing of 4-arc-minute (about 7.2 km at the equator) and saved at 16-arc-minute (about 28.8 km at the equator) resolution. This resolution may introduce large model diffusion effects if applied directly to the continental shelf, where the water depth is generally less than 100 m. The telescoped grids adopted in the MOST model are thus critical for wave transformation over the continental shelf, and for the inundation modeling at the coastline. Ideally, manipulation of β value will reduce the effects of diffusion and mimic the real-world dispersion through numerical dispersion.

3.3.2 Digital Elevation Model of Nikolski, Alaska

Lim et al. (2010) at the National Geophysical Data Center (NGDC) developed a 1-arc-sec digital elevation model of Nikolski, Alaska. The bathymetry was developed base on NOAA hydrographic survey soundings between 1910 and 1940, NGDC's multibeam swath sonar surveys in 2007, and NGDC ETOPO1 Global Relief Model. The topography in NGDC's DEM was based on USGS 2 arcsec NED DEM, NASA 1 arcsec SRTM, and ASTER 1 arcsec topographic DEM.

Lim et al. (2010) provided a detailed description of how these datasets were implemented in the DEM development for Nikolski. Most of the land elevation is obtained from NASA SRTM DEM, which is well known to have ±16 m of errors in vertical elevation. The model results computed using SRTM topography should be cautiously implemented in any tsunami forecast emergency, and need to be "flagged" in the forecast system.

3.3.3 Development of model grids

Development of an optimized tsunami forecast model for Nikolski began with the spatial extent merged bathymetric/topographic grids shown in **Figure 3 to 8**. Grid dimension extension and additional information were updated as needed and appropriate. A significant portion of the modeled tsunami waves, typically 4 to 10 hr of modeled

tsunami time, pass through the model domain without appreciable signal degradation. **Table 2** provides specific details of both reference and tsunami forecast model grids, including extents and complete input parameter information for the model runs is provided in **Appendix 1**.

Figure 3 shows the coverage of A grid with a space resolution of 30 arc seconds, which was employed by both the optimized tsunami forecast model and the reference model. This grid is obtained from the ETOPO 1 global relief database. The eastern boundary of A grid is specified at 177.5°W, and the southern boundary is set at 50°N extending south of the Aleutian Trench. It's recommended that the ocean boundary of A grid be placed at a water depth greater than 1,500 m to allow a smooth transition from the 4 arcmin tsunami propagation database where the waves are assumed to be linear. This A grid is also used in Nikolski forecast model 2 to provide more accurate computation of the tsunami propagation along the shallow coasts in the Aleutians with broader coverage and higher grid resolution (**Figure 4**). The modeling results in the next section show this implementation resulted high consistency between the forecast model and the reference model. The red box in Figure 3 indicates the coverage of the A grid in forecast model 1, which sets its western boundary at 170.5°W.

Figure 5 and **Figure 6** show the bathymetry and topography of B grid for the optimized forecast model and the reference model. The two grids have the same model extent (Table 2) with different grid resolutions, 12 arc second for the forecast model and 3 arc second for the reference model. Both grids were obtained from the Nikolski 1-arc-sec DEM developed by NGDC (Lim et al., 2010). The southern boundary of the B grid is located on the land side of the Aleutian trench, approximately 200 km offshore of the Pacific coastline of Umnak Island with a maximum water depth of 2,000 m. Nikolski is placed at the center of B grid to minimize the numerical errors introduced by the connecting boundary between grids A and B. The high grid resolution clearly shows more rugged bathymetric contours offshore.

To satisfy the model computing time requirement, the C grid of the optimized forecast model was developed at a grid resolution of 2 arcsec in x direction (37 m at latitude 53°N) and 1 arcsec in y direction (~ 31 m). Covering the same area, the reference model uses a 1 arc sec grid resolution for both x and y directions (19 m in x direction at latitude 53°N and 37 m in y direction) (**Figure 7 and 8**). The Nikolski C grid provides full coverage of the Nilkolski residential area, and the vicinity along 10 km coastline centered at Nikolski Village. Both grids were built from the Nikolski 1-arc-sec DEM developed by NGDC (Lim et al., 2010) with the maximum water depth of 60 m located at the northwestern boundary. As mentioned earlier, the topography built in Nikolski DEM was mostly derived from the NASA SRTM data, some of the land features, especially the mountain lakes, were not correctly reproduced. Most of the lakes were given by the elevation of the water surface with unknown water depth. As the Umnak Lake may potentially affect the tsunami flow on land when Nikolski is inundated, this study has manually change the topographic of the Umnak Lake area to a consistent water depth 33 m, which is the water depth that can theoretically minimize the model instability based on CFL condition (Burwell et al., 2007). It is worth noting that the Nikolski forecast models need to be improved when better topography becomes available.

4. Results and Discussion

4.1 Model validation

The small A grid coverage makes forecast model 1 satisfy the running time criterion, and give agreeable results to forecast model 2 and the reference model for the first several waves. For the three historical events (Table 3), the computed maximum wave amplitudes have less than 10% difference among three models (Table 4). Model results from forecast model 1 show some discrepancies in the late waves when comparing to the other two models, while results computed from the latter two models are highly consistent in terms of wave amplitudes, wave period, and phase.

The 2009 Samoa tsunami was triggered by a complex rupture process that probably had involved one Mw 8.1 earthquake in outer trench and two major Mw 7.8 interplate underthrusting subevents (Lay et al., 2010). Beavan et al. (2010) suggested that an outer rise earthquake was probably triggered by a thrust fault event, and they both contributed to the tsunami. NOAA's experimental tsunami forecast system constrained a tsunami source using three deep-ocean tsunameters that recorded distinct signal of the 2009 Samoa tsunami (Zhou et al., 2012). This tsunameter-constrained source clearly indicated that the tsunami source was a combination of an outer-rise event and a thrust-fault event. The records of this tsunami at Nikolski tide station indicated the tsunami wave reached a maximum amplitude of 13.8 cm at 14 hour 15 minutes after the earthquake (four hour 45 minutes after the tsunami arrived at Nikolski tide station). Both forecast models and the reference model underestimated the maximum wave amplitude, as shown in Table 3. The tsunameter-inversed source may need to be further improved for a better comparison. It is also worth noting that the noise level in the Nikolski tide gage records is high (Figure 10g), which normally leads to poor model/data comparison. The computed maximum wave amplitude and maximum flow speed in all three models show consistent results, but the forecast model 2 and reference model predicted slightly larger wave amplitude in the south of Nikolski Bay, especially near the Nikolski Village (Figure 8 a-f). Although a same C grid is used in both forecast model 1 and 2, the flow speed near the shallow area offshore of Nikolski Village indicates a larger A grid indeed introduces different wave dynamics in Nikolski Bay.

The 2011 Japan tsunami is the largest event that was ever recorded by the Nikolski tide gage. The maximum tsunami amplitude reached 81 cm above mean sea level. The tsunami source of this event was constrained in real time using two closest tsunameters provided accurate model forecast for more than 32 coastal communities five hours before the tsunami arrival in Hawaii (Tang et al., 2012). The hindcast inundation modeling using the same tsunami source indicated a 85% model accuracy in predicting the flooded areas in the near field along the east coastline of Japan (Wei et al., 2012). Figure 9 shows both the forecast model 1 and 2 and reference model gave good agreement for the first four waves, but spiked up for the fifth wave that resulted 30-40% overestimate of the maximum wave amplitude. This inconsistency between model and measurements is currently under investigation. Figure 9 also indicates that the maximum tsunami water level is close to 2 m near Nikolski Village, but had no major inundation impact on the residents or the coastline. The model shows the maximum flow speed is 0.5 to 1 m/s in the bay, and may have reached 2 m/s at the shallow area offshore of Nikolski Village.

The local residents should be warned with these high-speed tsunami-induced flow as fishing is one of the main economical activities that serve the community.

The 2011 Amutka Pass tsunami triggered by an Mw 7.3 earthquake was reported by several deep-ocean tsunameters with less than 2 cm peak. A real-time inversion using these deep-ocean measurements estimated an average slip of 0.26 m over a 100 km × 100 km rupture area. The model results using this source gave good comparison with the recorded data. All models correctly reproduced the arrival time and the waves up to three hours after the arrival, and the predicted maximum wave amplitude gave a <10% difference among all models. The late waves (after five hours) computed using forecast model 1 decays more rapidly than forecast model 2 and reference model.

The results from the forecast model 2 and the reference model show high consistency in wave amplitude, wave period, arrival time, and current speed. However, the use of forecast model 2 is not most efficient for forecast purpose due to its long running time. In comparison to forecast model 2, forecast model 1 can reduce the running time by almost 10 times, but may introduce extra computational error by 10 to 30%. One solution to make the forecast efficient and accurate is to adopt both forecast models in the forecast system, and use forecast model 2 to confirm or improve forecast model 1 results when more time is allowed to provide forecast products.

4.2 Model stability testing using synthetic scenarios

Model stability testing using synthetic scenarios provides important case studies to test the robustness, durability, and efficiency of the developed models from different perspectives:

1. Synthetic scenarios examine the developed models with mega tsunamis to guarantee model stability. These model tests ensure the efficiency of the forecast model during a catastrophic event.

2. Synthetic scenarios also examine the developed models with medium tsunamis to guarantee model stability under smaller wave conditions. These model tests ensure the efficiency of the forecast model during a moderate event.

3. Synthetic scenarios examine the developed models with negligible tsunami waves to guarantee the modeling results are not interfered by the numerical noises.

4. The synthetic scenarios were selected in such way that at least one from each potential tsunami source zone is tested. These cases are used to examine the reliability of the developed models in response to the directionality of tsunami waves.

Table 5 summarized all the synthetic scenarios (plotted in **Figure 2**) used in the present model testing. All scenarios are artificially constructed using a combination of the unit sources, shown as black boxes. Table 5 gives the details of unit source and the coefficients for a total of 21 scenarios, including 19 with magnitude 9.3, one with magnitude 7.5 and one micro-wave scenario. All scenarios were tested in forecast model

1, forecast model 2, and reference model for 24-hour model runs. All tests were successful to maintain the model stability throughout the run.

The M_w 9.3 synthetic scenarios, ACSZ 06-15, ACSZ 16-25, and ACSZ 22-31, in the western Alaska-Aleutian subduction zone are among the sources that may generate the most catastrophic tsunami waves to Nikolski. **Figure 12-14** show all three scenarios have produced serious flooding along the coastline of Nikolski. The tsunami flow could penetrate the residential village and reach the Umnak Lake, which rests on a higher ground behind the village. ACSZ 16 to 25 represents a worst-case scenario of the tsunami hazards in Nikolski, which over-floods the entire village with tsunami water level up to 13 m above mean high water. The maximum tsunami wave amplitude at the tide gage can reach 10.5 m (Table 6), and the tide gage sensor may be exposed when large wave troughs pass due to the shallow water depth there. **Figure 13** shows the tsunami flooding will occur along the entire coastline in Unmak Bay, and at the embayment in the north of Nikolski the water level may reach up to 17 m above mean high water. The flow speed induced by the ACSZ 16-25 scenario is as large as 10 m/s over the Nikolski Village. The Umnak Bay will be saturated with strong currents at similar flow speed. The computational results from forecast model 2, as well as the reference model, indicates the large waves (3 to 4 m) may sustain for more than half a day after the tsunami is generated. The synthetic scenario ACSZ 06 to 15 also caused flooding in Nikolski Village, and induced high tsunami waves that can reach the Umnak Lake. The wave amplitude at the tide station, however, is approximately half as much in comparison with ACSZ 16 to 25. In the cases of ACSZ 06 to 15 and ACSZ 22 to 31, the time series at tide gage location computed from forecast model 1 agrees well with the results obtained in forecast model 2 and reference model for the first 4 to 5 waves, but shows discrepancies in phase and wave period thereafter. These differences start at an earlier time, one and half hours after the tsunami is generated, in the scenario ACSZ 16 to 25. It indicates that enlarging the coverage of A grid with higher grid resolution will provide more accurate simulation of the wave dynamics on the shallow shelf along the Aleutian Islands. The water level in Nikolski is generally less than 1.5 m when the tsunami is generated by M_w 9.3 earthquake in the subduction zones along east Alaska, Canada and Cascadia, as in **Figure 15 and 16**. However, it is worth noting that in these scenarios the trailing waves near Nikolski decay very slowly, indicating strong wave oscillation in Umnak Bay. As a result, the maximum wave amplitude may arrive hours later – for instance, the maximum water level occurred at seven hours after tsunami arrival in both scenarios (**Figure 15g and 16g**). The wave period is also increasing in the late waves. In case of real event, the tsunami warning along coastline of Nikolski needs to be sustained for at least half day due to local wave oscillations.

Radiation of tsunami energy in the ocean basin is affected by the tsunami source alignment, as well as the bathymetry (Titov et al., 2005; Grilli et al., 2007). The synthetic M_w 9.3 scenarios (CSSZ 01 to 10 and CSSZ 37 to 46) using northern segment of Central-South Subduction Zone could only produce minor water level increase along Nikolski's coastline. The time series at the tide gage for the two cases shows the maximum water level is less than 40 cm. In the case of CSSZ 01 to 10, the discrepancy of the maximum water level between forecast models and reference model is mainly due to the short run time in the reference model, while the maximum waves arrive at 23 to 24 hours after the

tsunami generation (14 to 15 hours after the tsunami waves arrive at the tide gage), as seen from the forecast model results in Figure 16g. Once again, it is a strong indication of long duration of tsunami impact along the coastline of Nikolski. In comparison to the other two models (forecast model 2 and reference model), , forecast model 1 tends to underestimate the maximum water level when it arrives with the late waves (**Figure 17**). The fault orientation in the cases of CSSZ 89 to 98 and CSSZ 102 to 111 is able to radiate tsunami energy more effectively towards the Aleutians. The highest tsunami water level due to these M_w 9.3 sources may reach 2.9 m at the Nikolski tide gage (Figure 18 and 19), even though these tsunami sources are approximately 15,000 km away.

Another source region that may generate serious tsunami impact to coasts of Nikolski is the Kamchatka-Yap-Mariana-Izu-Bonin source zone. The northern segment of KISZ (KISZ 01 to 10) is able to generate tsunami waves as high as 3 m at Nikolski tide gage (**Figure 21**). The tsunami waves generated by this synthetic source can approach Nikolski from both the Bering Sea and the Pacific Ocean along the Aleutian Island chain. Consequently, the coastal communities in the Aleutians are vulnerable to tsunamis generated in the northern tip of KISZ (Wei, 2012). These tsunamis can strike Nikolski harder than those originating east of the ACSZ. The funneled bathymetry may direct the waves, after crossing the Bering Sea from the west, to Nikolski. The tsunamis generated from the central segment of KISZ (KISZ 22 to 31) raises the water level up to 1.5 m, about half of that in case ACSZ 01 to 10 (**Figure 22**). The southern segment of this source region (KISZ 56 6o 65 and KISZ 32 to 41) may produce tsunami waves as high as 3.2 m in Nikolski, and creates limited flooding to the community at Nikolski (**Figure 23 and 24**). The peak-to-trough wave heights in both cases are greater than 4 m, representing strong tsunami energy that can still result in significant impact to the fishing boats, local ecology and coastal structures. Different from the tsunamis generated in eastern ACSZ or CSSZ, the maximum waves of tsunamis generated in the KISZ usually arrive within the first group of large waves, say three to four hours of the tsunami arrival. Although the late waves cannot be ignored, the first group of large waves may be more important to be alerted for the coastal community at Nikolski.

Many of the synthetic scenarios are shown to highlight the important characteristics of late waves. The wave amplitude did not reach its maximum until almost 14 or 15 hours after the first wave arrived at Nokolski tide gage. When comparing the modeling results between the forecast model 2 and the reference model for the first eight hours, one can observe an excellent agreement in computed wave amplitude, flow speed, and time series at the tide gage. These synthetic scenarios stress on the need of retaining the tsunami warning or watch for more than 24 hours for the coasts of NIkolski during a real tsunami event. The main discrepancies between forecast model 1 and the other two models are mostly in the late waves, where A grid coverage and grid resolution plays a major role in the numerical simulation of tsunami propagation along Aleutian Islands.

Excellent agreement was also found between the forecast model 2 and reference model for many other synthetic scenarios, such as EPSZ 06 to 15, MOSZ 01 to 10, NGSZ 03 to 12, NTZ 30 to 39, NVSZ 28 to 37 and RNSZ 12 to 21, that represent a Mw 9.3 earthquake-generated tsunami waves from major subduction zones in the Pacific (**Figure**

25 to 30). The model results show that EPSZ 06 to 10 and MOSZ 01 to 10 may produce a maximal water elevation of 1.8 m at Nikolski tide gage, and the minimum water level can reach as high as 1 m at the Nikolski tide gage (Table 6).

The synthetic scenario of magnitude 7.5, NTSZ b36, introduces only up to 3.2 cm wave amplitude along the shoreline of NIkolski, and 1.8 cm at the tide gage. Both the forecast model 2 and reference model show good model consistency and stability in terms of maximum wave amplitudes, flow speed and the time series at the tide gage (**Figure 31**). The micro scenario EPSZ b19 is very useful in testing the model stability under the conditions of negligible wave. From the computed maximum wave amplitude (Figure **), one can see that the water elevation at the oceanfront is only on the order of 10^{-4} m, and the computed time series from both models have excellent match. The two models show small difference mostly in the marshy area and narrow marinas, where the reference model describes many more local bathymetric and topographic features that result in more wave dynamics, which, on the other hand, may also introduce some numerical abnormality to the model. This issue is being further investigated.

5. Summary and conclusions

Nikolski, Alaska is a coastal community at the northern Umnak Island. Nikolski is not known of its vulnerability to potential tsunami hazards, which pose long-standing challenges for the coastal communities on how to protect their lives and properties. Tsunami forecast and hazard assessment in Nikolski, however, remains significantly understudied, probably due to the minor impact and infrequent occurrence of tsunamis in Nikolski's history.

A tsunami forecast model is presently developed for the community of Nikolski, Alaska. The developed model is being implemented into NOAA's Short-term Inundation Forecast of Tsunamis (SIFT) to provide real-time modeling forecasts of tsunami wave characteristics, runup and inundation along Nikolski's coastline. Discussion of the details of each individual components of the forecast model, including the bathymetry and topography, the basic model setup, and the model parameters are provided in the report. The forecast model employs grids as fine as 2 aecsrc (37 m) in x axis and 1 arcsec (37 m) in y axis and can accomplish a four-hour simulation, after tsunami arrival, in 12.4 minutes of computer CPU time. This study developed two forecast models, forecast model 1 and forecast model 2, that employs an A grid with different coverage and grid resolution. Due to lack of higher resolution DEM, a reference model was developed with similar grid resolution, using grids as fine as 1 arcsec (19 m in x axis and 31 m in y axis) , to provide reference results basis for performance evaluation of the forecast model. Model validation and tests indicate that forecast model 2 and reference model show high consistency in the modeling results, however forecast model 1 shows up to 30% difference in the maximum wave amplitude. Forecast model 1 also shows slight difference in wave period and phase speed, mainly in the late waves. It is recommended that both forecast model 1 and 2 to be implemented in the forecast system for both forecast speed and forecast accuracy.

Nikolski tide station has recorded several tsunamis since its establishment in 2006. The 2009 Samoa, 2011 Japan and 2011 Amutka Pass tsunamis were used for model

validation. The models correctly predicted the arrival time and first few waves. The model accuracies of the maximum wave amplitude at the tide station are 59% (large background noise), 65%, and 90% for the three events, respectively. The model results of the three events indicated that the 2011 Japan tsunami might have brought strong tsunami up to 2 m/s to offshore of Nikolski, while the flow speed of the other two tsunamis were smaller than 0.5 m/s. The results from both the forecast model (especially forecast model 2) and the reference model showed excellent agreement in wave amplitude, wave period, arrival time, and current speed.

A total of 21 synthetic scenarios, including 19 synthetic events generated by an M_w 9.3 source, one synthetic event due to an M_w 7.5 source, and one micro-size tsunami, were used to examine the stability of the developed forecast model and reference model for Nikolski. The synthetic scenarios were selected in such way that at least one from each of the major source zones in the Pacific is tested. Both the forecast models and reference model give stable results for all synthetic scenarios representing tsunami waves from different source locations and different directionalities. Other than testing the model stability, these synthetic scenarios are also useful to summarize some common the characteristics of tsunami waves generated from these source zones.

1. A M_w 9.3 earthquake offshore of the Pacific coast of Umnak Island (ACSZ 16 to 25) may cause catastrophic tsunami for the small community in Nikolski. The modeling results show such a tsunami would inundate the entire Nikolski Village with waves as high as 13 m. Tsunamis caused by earthquake of same magnitude in the Aleutians (ACSZ 06 to 15 and ACSZ 22 to 31) may flood part of the Nikolski Village.

2. Other scenarios are unlikely to cause major flooding at the waterfront of Nikolski, They are less threatening, but the high seas and rapid flow may still cause damages to coasts along Umnak Bay in terms of fishing activity, ecology system, as well as coastal facilities.

3. Tsunami waves inside Umnak Bay and near Nikolski are featured with long-time wave oscillation, which may amplify the wave amplitude and result in hours of delay to the arrival of the maximum wave. As such, the tsunami warning should be upheld for at least half day after the first arrival of the tsunami waves.

4. All model results indicate that Nikolski is likely to be the place that is affected the most by the tsunami within the Umnak Bay. Its location in southeast corner of the Umnak Bay is most effective to trap the sunami energy, in other words, being a node of the resonant tsunami waves in the bay. The tsunami wave resonance inside the Umnak Bay is currently under investigation.

All model validation and stability tests demonstrated that the developed tsunami forecast model and reference model for Nikolski, Alaska, are robust and efficient for their implementation into both the short-term real-time tsunami forecast system and long-term tsunami inundation investigations, although the models needs to be further updated when more accurate DEMs become available. The optimized forecast model developed for Nikolski provides a four-hour forecast of first wave arrival, amplitudes, and inundation

within 12.4 minutes based on testing with available historical and synthetic events as presented in this report.

6. Acknowledgement

Funding for this publication and all work leading to development of a tsunami forecast model for NIkolski, Alaska was provided by the National Oceanic and Atmospheric Administration. This publication was partially funded by the Joint Institute for the Study of the Atmosphere and Ocean (JISAO) under NOAA Cooperative Agreement NO. NA17RJ1232, JISAO Contribution No. ****. This is PMEL Contribution No. ****.

7. References:

Beavan, J., Wang, X., Holden, C., Wilson, K., Power, K., Prasetya, G., Bevis, M. and Kautoke, R. (2010). Near-simultaneous great earthquakes at Tongan megathrust and outer rise in September 2009, Nature, 466, 959–963.

Burwell, D., E. Tolkova, and A. Chawla (2007), Diffusion and dispersion characterization of a numerical tsunami model, *Ocean Modeling*, 19, 10-30.

Hyers, F.M. Jr. (1959): Geology of Umnak and Bogoslof Islands, Aleutian Islands, Alaska – investigations of Alaskan Volcanoes. Geological Survey Bulletin 1028-L, 365 pp.

Gica, E., M. Spillane, V.V. Titov, C. Chamberlin, and J.C. Newman (2008), Development of the forecast propagation database for NOAA's Short-term Inundation Forecast for Tsunamis (SIFT). NOAA Tech. Memo. OAR PMEL-139, 89 pp.

Grilli, S.T., M. Ioualalen, J. Asavanant, F.Y. Shi, J.T. Kirby, and P. Watts (2007). Source constraint and model simulation of the December 26, 2004, Indian Ocean tsunami, *J. Waterway Port Coastal Ocean Eng.*, 133(6), 414-428.

Lay, T., Ammon, C.J., Kanamori, H., Rivera, L., Koper, K.D. and Hutko, A.R. (2010). The 2009 Samoa-Tonga great earthquake triggered doublet, Nature, 466, 964-968, doi:10.1038/nature09214.

Lim, E., L.A. Taylor, B.W. Eakins, K.S. Carignan, P.R. Grothe, R.J. Caldwell, and D.Z. Friday (2010). Digital elevation model of Nikolski, Alaska: procedures, data sources and analysis – prepared for the Pacific Marine Environmental Laboratory (PMEL) NOAA Center for Tsunami Research by the NOAA National Geophysical Data Center (NGDC), 24p.

Synolakis, C.E., E.N. Bernard, V.V. Titov, U. Kânoğlu, and F.I. González (2008): Validation and verification of tsunami numerical models. *Pure Appl. Geophys.*, *165*(11–12), 2197–2228.

Tang, L., V. V. Titov, and C. D. Chamberlin (2009), Development, testing, and applications of site-specific tsunami inundation models for real-time forecasting, *J. Geophys. Res.*, 114, C12025, doi:10.1029/2009JC005476.

Tang, L., V. V. Titov, E. Bernard, Y. Wei, C. Chamberlin, J. C. Newman, H. Mofjeld, D. Arcas, M. Eble, C. Moore, B. Uslu, C. Pells, M. C. Spillane, L. M. Wright, and E. Gica (2012): Direct energy estimation of the 2011 Japan tsunami using deep-ocean pressure measurements. J. Geophys. Res., doi:10.1029/2011JC007635, in press

Tang, L., V.V. Titov, E. Bernard, Y. Wei, C. Chamberlin, J.C. Newman, H. Mofjeld, D. Arcas, M. Eble, C. Moore, B. Uslu, C. Pells, M.C. Spillane, L.M. Wright, and E. Gica (2012): Direct energy estimation of the 2011 Japan tsunami using deep-ocean pressure measurements. J. Geophys. Res., 117, C08008, doi: 10.1029/2011JC007635.

Tang, L., V.V. Titov, Y. Wei, H.O. Mofjeld, M. Spillane, D. Arcas, E.N. Bernard, C. Chamberlin, E. Gica, and J. Newman (2008): Tsunami forecast analysis for the May 2006 Tonga tsunami. *J. Geophys. Res.*, *113*, C12015, doi: 10.1029/2008JC004922.

Titov, V.V. (2009): Tsunami forecasting. Chapter 12 in *The Sea, Volume 15: Tsunamis*, Harvard University Press, Cambridge, MA and London, England, 371–400.

Titov, V.V, E. Gica, M. Spillane, Y. Wei, C. Moore, H. Zhou and R. Weiss (2009), Tsunami hazard assessment for the U.S. East Coast based on generation, propagation and inundation modeling, *NCTR Letter Report to the Nuclear Regulatory Commission*, 117pp.

Titov, V., and F.I. González (1997): Implementation and testing of the Method of Splitting Tsunami (MOST) model. NOAA Tech. Memo. ERL PMEL-112 (PB98-122773), NOAA/Pacific Marine Environmental Laboratory, Seattle, WA, 11 pp.

Titov, V.V., F.I. González, E.N. Bernard, M.C. Eble, H.O. Mofjeld, J.C. Newman, and A.J. Venturato (2005a): Real-time tsunami forecasting: Challenges and solutions. Nat. Hazards, 35(1), Special Issue, U.S. National Tsunami Hazard Mitigation Program, 41–58.

Titov, V.V., A.B. Rabinovich, H.O. Mofjeld, R.E. Thomson, and F.I. González (2005b), The global reach of the 26 December 2004 Sumatra Tsunami. *Science*. doi: 10.1126/science.1114576.

Wei, Y. (2012): A Tsunami Forecast Model for Unalaska, Alaska. NOAA OAR Special Report, PMEL Tsunami Forecast Series: Vol. 10, in press.

Wei, Y., E. Bernard, L. Tang, R. Weiss, V. Titov, C. Moore, M. Spillane, M. Hopkins, and U. Kânoğlu (2008): Real-time experimental forecast of the Peruvian tsunami of August 2007 for U.S. coastlines. *Geophys. Res. Lett.*, *35*, L04609, doi: 10.1029/2007GL032250.

Wei, Y., C. Chamberlin, V.V. Titov, L. Tang, and E.N. Bernard (2012): Modeling of 2011 Japan Tsunami - lessons for near-field forecast, *Pure Appl. Geophys*., doi: 10.1007/s00024-012-0519-z, in press.

Wei, Y., U.S. ten Brink, and B. Atwater (2011): Tsunami sources that might explain the catastrophic overwash of Anegada, British Virgin Islands, between 1650 and 1800. *Journal*

of Geophysical Research, in preparation.

Zhou, H., Wei, Y. and Titov, V.V. (2012). Dispersive modeling of the 2009 Samoa tsunami, Geophys. Res. Lett., in review.

Forecast model 1 .in file:

```
0.005    Minimum amplitude of input offshore wave (m)
1.0  Input minimum depth for offshore (m)
0.1  Input "dry land" depth for inundation (m)
0.0009   Input friction coefficient (n**2)
1    let a and b run up
300.0    blowup limit
1    input time step (sec)
24000    input amount of steps
3    Compute "A" arrays every n-th time step, n=
1    COmpute "B" arrays every n-th time step, n=
30   Input number of steps between snapshots
0    ...Starting from
1    ...saveing grid every n-th node, n=
nikolski1_run2d/niko1_Agrid_1min.most
nikolski1_run2d/niko_Bgrid_12s.most
nikolski1_run2d/niko_Cgrid_x2s_y1s.most
./
./
1 1 1 1  NetCDF output for A, B, C, SIFT
1    Timeseries locations:
3 109 105nikolski1191.13   52.941111depth m: 2.3  NK1
  Nikolski, AK
```

Forecast model 2 .in file:

```
0.005    Minimum amplitude of input offshore wave (m)
1.0  Input minimum depth for offshore (m)
0.1  Input "dry land" depth for inundation (m)
0.0009   Input friction coefficient (n**2)
1    let a and b run up
300.0    blowup limit
1    input time step (sec)
28800    input amount of steps
2    Compute "A" arrays every n-th time step, n=
1    COmpute "B" arrays every n-th time step, n=
30   Input number of steps between snapshots
0    ...Starting from
1    ...saveing grid every n-th node, n=
nikolski2_run2d/niko2_Agrid_30s.most
nikolski2_run2d/niko_Bgrid_12s.most
nikolski2_run2d/niko_Cgrid_x2s_y1s.most
./
./
1 1 1 1  NetCDF output for A, B, C, SIFT
1    Timeseries locations:
3 109 105nikolski2191.13   52.941111depth m: 2.3  NK2
  Nikolski, AK
```

Reference model .in file:

```
0.005 Minimum amplitude of input offshore wave (m)
1.0  Input minimum depth for offshore (m)
0.1   Input "dry land" depth for inundation (m)
0.0009 Input friction coefficient (n**2)
1     let a and b run up
300.0 blowup limit
0.3   input time step (sec)
96000 input amount of steps
6     Compute "A" arrays every n-th time step, n=
1     COmpute "B" arrays every n-th time step, n=
120    Input number of steps between snapshots
0   ...Starting from
1     ...saveing grid every n-th node, n=
nikolski_run2d/niko_rim_Agrid.most
nikolski_run2d/niko_rim_Bgrid.most
nikolski_run2d/niko_rim_Cgrid.most
./
./
1 1 1 1
1    Timeseries locations:
3 217 105nikolski2191.13   52.941111depth m: 2.3  NK
  Nikolski, AK
```

Figures:

Figure 1. (a) Aerial view of Nikolski, Alaska and the location of the Nikolski tide station. (b) Land view of Nikolski, Alaska and location of the Nikolski tide station.

Figure 2. Historical tsunami events that have affected Nikolski, Alaska. The earthquake location are indicated by ●. The black boxes are the tsunami propagation unit sources (Gica et al., 2008). Also included are model scenarios used in model validation and stability testing.

Figure 3. A-grid bathymetry and topography for the reference model, where the black boxes indicate the coverage of B grid and C grid.

Figure 4. A-grid bathymetry and topography for the forecast models. reference model, where the red box indicates the coverage of A grid of forecast model 1, and the black boxes indicate the coverage of B grid and C grid.

Figure 5. B-grid bathymetry and topography for the reference model, where the black boxes indicate the coverage of C grid. The red solid circle labels the location of the Nikolski tide station.

Figure 6. B-grid bathymetry and topography for both forecast models, where the black boxes indicate the coverage of C grid. The red solid circle labels the location of the Nikolski tide station.

Figure 7. C-grid bathymetry and topography for the reference model, where the red solid circle labels the location of the Nikolski tide station.

Figure 8. C-grid bathymetry and topography for both forecast models, where the red solid circle labels the location of the Nikolski tide station.

Figure 9. Modeling results for the 29 September, 2009 Samoa tsunami. (a) Maximum wave amplitude in the C grid computed from forecast model 1; (b) Maximum flow speed in the C-grid computed from forecast model 1; (c) Maximum wave amplitude in the C grid computed from forecast model 2; (d) Maximum flow speed in the C-grid computed from forecast model 2; (e) Maximum wave amplitude in the C grid computed from the reference model; (b) Maximum flow speed in the C-grid computed from reference model. (e) Comparison of the computed time series between observation, forecast models and reference model at the Nikolski tide station.

Figure 10. Modeling results for the 11 March, 2011 Japan tsunami. (a) Maximum wave amplitude in the C grid computed from forecast model 1; (b) Maximum flow speed in the C-grid computed from forecast model 1; (c) Maximum wave amplitude in the C grid computed from forecast model 2; (d) Maximum flow speed in the C-grid computed from forecast model 2; (e) Maximum wave amplitude in the C grid computed from the reference model; (b) Maximum flow speed in the C-grid computed from reference model. (e) Comparison of the computed time series between observation, forecast models and reference model at the Nikolski tide station.

Figure 11. Modeling results for the 24 June, 2011 Amutka Pass event. (a) Maximum wave amplitude in the C grid computed from forecast model 1; (b) Maximum flow speed in the C-grid computed from forecast model 1; (c) Maximum wave amplitude in the C grid computed from forecast model 2; (d) Maximum flow speed in the C-grid computed from forecast model 2; (e) Maximum wave amplitude in the C grid computed from the reference model; (b) Maximum flow speed in the C-grid computed from reference model. (e) Comparison of the computed time series between observation, forecast models and reference model at the Nikolski tide station.

Figure 12. Modeling results for the ACSZ 06-15 scenario. (a) Maximum wave amplitude in the C grid computed from forecast model 1; (b) Maximum flow speed in the C-grid computed from forecast model 1; (c) Maximum wave amplitude in the C grid computed from forecast model 2; (d) Maximum flow speed in the C-grid computed from forecast model 2; (e) Maximum wave amplitude in the C grid computed from the reference model; (b) Maximum flow speed in the C-grid computed from reference model. (e) Comparison of the computed time series between forecast models and reference model at the Nikolski tide station.

Figure 13. Modeling results for the ACSZ 16-25 scenario. (a) Maximum wave amplitude in the C grid computed from forecast model 1; (b) Maximum flow speed in the C-grid computed from forecast model 1; (c) Maximum wave amplitude in the C grid computed from forecast model 2; (d) Maximum flow speed in the C-grid computed from forecast model 2; (e) Maximum wave amplitude in the C grid computed from the reference model; (b) Maximum flow speed in the C-grid computed from reference model. (e) Comparison of the computed time series between forecast models and reference model at the Nikolski tide station.

Figure 14. Modeling results for the ACSZ 22-31 scenario. (a) Maximum wave amplitude in the C grid computed from forecast model 1; (b) Maximum flow speed in the C-grid computed from forecast model 1; (c) Maximum wave amplitude in the C grid computed from forecast model 2; (d) Maximum flow speed in the C-grid computed from forecast model 2; (e) Maximum wave amplitude in the C grid computed from the reference model; (b) Maximum flow speed in the C-grid computed from reference model. (e) Comparison of the computed time series between forecast models and reference model at the Nikolski tide station.

Figure 15. Modeling results for the ACSZ 50-59 scenario. (a) Maximum wave amplitude in the C grid computed from forecast model 1; (b) Maximum flow speed in the C-grid computed from forecast model 1; (c) Maximum wave amplitude in the C grid computed from forecast model 2; (d) Maximum flow speed in the C-grid computed from forecast model 2; (e) Maximum wave amplitude in the C grid computed from the reference model; (b) Maximum flow speed in the C-grid computed from reference model. (e) Comparison of the computed time series between forecast models and reference model at the Nikolski tide station.

Figure 16. Modeling results for the ACSZ 56-65 scenario. (a) Maximum wave amplitude in the C grid computed from forecast model 1; (b) Maximum flow speed in the C-grid computed from forecast model 1; (c) Maximum wave amplitude in the C grid computed

from forecast model 2; (d) Maximum flow speed in the C-grid computed from forecast model 2; (e) Maximum wave amplitude in the C grid computed from the reference model; (b) Maximum flow speed in the C-grid computed from reference model. (e) Comparison of the computed time series between forecast models and reference model at the Nikolski tide station.

Figure 17. Modeling results for the CSSZ 01-10 scenario. (a) Maximum wave amplitude in the C grid computed from forecast model 1; (b) Maximum flow speed in the C-grid computed from forecast model 1; (c) Maximum wave amplitude in the C grid computed from forecast model 2; (d) Maximum flow speed in the C-grid computed from forecast model 2; (e) Maximum wave amplitude in the C grid computed from the reference model; (b) Maximum flow speed in the C-grid computed from reference model. (e) Comparison of the computed time series between forecast models and reference model at the Nikolski tide station.

Figure 18. Modeling results for the CSSZ 37-46 scenario. (a) Maximum wave amplitude in the C grid computed from forecast model 1; (b) Maximum flow speed in the C-grid computed from forecast model 1; (c) Maximum wave amplitude in the C grid computed from forecast model 2; (d) Maximum flow speed in the C-grid computed from forecast model 2; (e) Maximum wave amplitude in the C grid computed from the reference model; (b) Maximum flow speed in the C-grid computed from reference model. (e) Comparison of the computed time series between forecast models and reference model at the Nikolski tide station.

Figure 19. Modeling results for the CSSZ 89-98 scenario. (a) Maximum wave amplitude in the C grid computed from forecast model 1; (b) Maximum flow speed in the C-grid computed from forecast model 1; (c) Maximum wave amplitude in the C grid computed from forecast model 2; (d) Maximum flow speed in the C-grid computed from forecast model 2; (e) Maximum wave amplitude in the C grid computed from the reference model; (b) Maximum flow speed in the C-grid computed from reference model. (e) Comparison of the computed time series between forecast models and reference model at the Nikolski tide station.

Figure 20. Modeling results for the CSSZ 102-111 scenario. (a) Maximum wave amplitude in the C grid computed from forecast model 1; (b) Maximum flow speed in the C-grid computed from forecast model 1; (c) Maximum wave amplitude in the C grid computed from forecast model 2; (d) Maximum flow speed in the C-grid computed from forecast model 2; (e) Maximum wave amplitude in the C grid computed from the reference model; (b) Maximum flow speed in the C-grid computed from reference model. (e) Comparison of the computed time series between forecast models and reference model at the Nikolski tide station.

Figure 21. Modeling results for the KISZ 01-10 scenario. (a) Maximum wave amplitude in the C grid computed from forecast model 1; (b) Maximum flow speed in the C-grid computed from forecast model 1; (c) Maximum wave amplitude in the C grid computed from forecast model 2; (d) Maximum flow speed in the C-grid computed from forecast model 2; (e) Maximum wave amplitude in the C grid computed from the reference model; (b) Maximum flow speed in the C-grid computed from reference model. (e)

Comparison of the computed time series between forecast models and reference model at the Nikolski tide station.

Figure 22. Modeling results for the KISZ 22-31 scenario. (a) Maximum wave amplitude in the C grid computed from forecast model 1; (b) Maximum flow speed in the C-grid computed from forecast model 1; (c) Maximum wave amplitude in the C grid computed from forecast model 2; (d) Maximum flow speed in the C-grid computed from forecast model 2; (e) Maximum wave amplitude in the C grid computed from the reference model; (b) Maximum flow speed in the C-grid computed from reference model. (e) Comparison of the computed time series between forecast models and reference model at the Nikolski tide station.

Figure 23. Modeling results for the KISZ 32-41 scenario. (a) Maximum wave amplitude in the C grid computed from forecast model 1; (b) Maximum flow speed in the C-grid computed from forecast model 1; (c) Maximum wave amplitude in the C grid computed from forecast model 2; (d) Maximum flow speed in the C-grid computed from forecast model 2; (e) Maximum wave amplitude in the C grid computed from the reference model; (b) Maximum flow speed in the C-grid computed from reference model. (e) Comparison of the computed time series between forecast models and reference model at the Nikolski tide station.

Figure 24. Modeling results for the KISZ 56-65 scenario. (a) Maximum wave amplitude in the C grid computed from forecast model 1; (b) Maximum flow speed in the C-grid computed from forecast model 1; (c) Maximum wave amplitude in the C grid computed from forecast model 2; (d) Maximum flow speed in the C-grid computed from forecast model 2; (e) Maximum wave amplitude in the C grid computed from the reference model; (b) Maximum flow speed in the C-grid computed from reference model. (e) Comparison of the computed time series between forecast models and reference model at the Nikolski tide station.

Figure 25. Modeling results for the EPSZ 06-15 scenario. (a) Maximum wave amplitude in the C grid computed from forecast model 1; (b) Maximum flow speed in the C-grid computed from forecast model 1; (c) Maximum wave amplitude in the C grid computed from forecast model 2; (d) Maximum flow speed in the C-grid computed from forecast model 2; (e) Maximum wave amplitude in the C grid computed from the reference model; (b) Maximum flow speed in the C-grid computed from reference model. (e) Comparison of the computed time series between forecast models and reference model at the Nikolski tide station.

Figure 26. Modeling results for the MOSZ 01-10 scenario. (a) Maximum wave amplitude in the C grid computed from forecast model 1; (b) Maximum flow speed in the C-grid computed from forecast model 1; (c) Maximum wave amplitude in the C grid computed from forecast model 2; (d) Maximum flow speed in the C-grid computed from forecast model 2; (e) Maximum wave amplitude in the C grid computed from the reference model; (b) Maximum flow speed in the C-grid computed from reference model. (e) Comparison of the computed time series between forecast models and reference model at the Nikolski tide station.

Figure 27. Modeling results for the NGSZ 03-12 scenario. (a) Maximum wave amplitude in the C grid computed from forecast model 1; (b) Maximum flow speed in the C-grid computed from forecast model 1; (c) Maximum wave amplitude in the C grid computed from forecast model 2; (d) Maximum flow speed in the C-grid computed from forecast model 2; (e) Maximum wave amplitude in the C grid computed from the reference model; (b) Maximum flow speed in the C-grid computed from reference model. (e) Comparison of the computed time series between forecast models and reference model at the Nikolski tide station.

Figure 28. Modeling results for the NTSZ 30-39 scenario. (a) Maximum wave amplitude in the C grid computed from forecast model 1; (b) Maximum flow speed in the C-grid computed from forecast model 1; (c) Maximum wave amplitude in the C grid computed from forecast model 2; (d) Maximum flow speed in the C-grid computed from forecast model 2; (e) Maximum wave amplitude in the C grid computed from the reference model; (b) Maximum flow speed in the C-grid computed from reference model. (e) Comparison of the computed time series between forecast models and reference model at the Nikolski tide station.

Figure 29. Modeling results for the NVSZ 28-37 scenario. (a) Maximum wave amplitude in the C grid computed from forecast model 1; (b) Maximum flow speed in the C-grid computed from forecast model 1; (c) Maximum wave amplitude in the C grid computed from forecast model 2; (d) Maximum flow speed in the C-grid computed from forecast model 2; (e) Maximum wave amplitude in the C grid computed from the reference model; (b) Maximum flow speed in the C-grid computed from reference model. (e) Comparison of the computed time series between forecast models and reference model at the Nikolski tide station.

Figure 30. Modeling results for the RNSZ 12-21 scenario. (a) Maximum wave amplitude in the C grid computed from forecast model 1; (b) Maximum flow speed in the C-grid computed from forecast model 1; (c) Maximum wave amplitude in the C grid computed from forecast model 2; (d) Maximum flow speed in the C-grid computed from forecast model 2; (e) Maximum wave amplitude in the C grid computed from the reference model; (b) Maximum flow speed in the C-grid computed from reference model. (e) Comparison of the computed time series between forecast models and reference model at the Nikolski tide station.

Figure 31. Modeling results for the NTSZ B36 scenario. (a) Maximum wave amplitude in the C grid computed from forecast model 1; (b) Maximum flow speed in the C-grid computed from forecast model 1; (c) Maximum wave amplitude in the C grid computed from forecast model 2; (d) Maximum flow speed in the C-grid computed from forecast model 2; (e) Maximum wave amplitude in the C grid computed from the reference model; (b) Maximum flow speed in the C-grid computed from reference model. (e) Comparison of the computed time series between forecast models and reference model at the Nikolski tide station.

Figure 32. Modeling results for the NPSZ B19 scenario. (a) Maximum wave amplitude in the C grid computed from forecast model 1; (b) Maximum flow speed in the C-grid computed from forecast model 1; (c) Maximum wave amplitude in the C grid computed

from forecast model 2; (d) Maximum flow speed in the C-grid computed from forecast model 2; (e) Maximum wave amplitude in the C grid computed from the reference model; (b) Maximum flow speed in the C-grid computed from reference model. (e) Comparison of the computed time series between forecast models and reference model at the Nikolski tide station.

Tables:

Table 1: Historical tsunami events that have affected Nikolski, Alaska.

Tables 2: MOST setup parameters for reference and forecast models for Nikolski, Alaska.

Tables 3: Tsunami sources of historical events that were recorded at Nikolski tide station and used for model validation.

Table 4: Table 4. Computed maximum wave amplitude at Nikolski tide station for historical events. The percentage in the parentesis is the model error of the maximum wave amplitude at the Nikolski tide gage, where the error = $(\eta_{model} - \eta_{obs}) / \eta_{obs} \times 100\%$. η_{model} is the computed maximum wave amplitude, and η_{obs} is the observed maximum wave amplitude.

Tables 5: Synthetic tsunami events in the Pacific.

Table 6: Computed maximum wave amplitude at Nikolski tide station for synthetic scenarios. The percentage in the parentesis is the error of the maximum wave amplitude at the Nikolski tide gage computed using the two forecast models in reference to the reference model, where the error = $(\eta_{fm} - \eta_{rm}) / \eta_{rm} \times 100\%$. η_{fm} is the computed maximum wave amplitude using the forecast models, and η_{rm} is the computed maximum wave amplitude using the reference model.

(a)

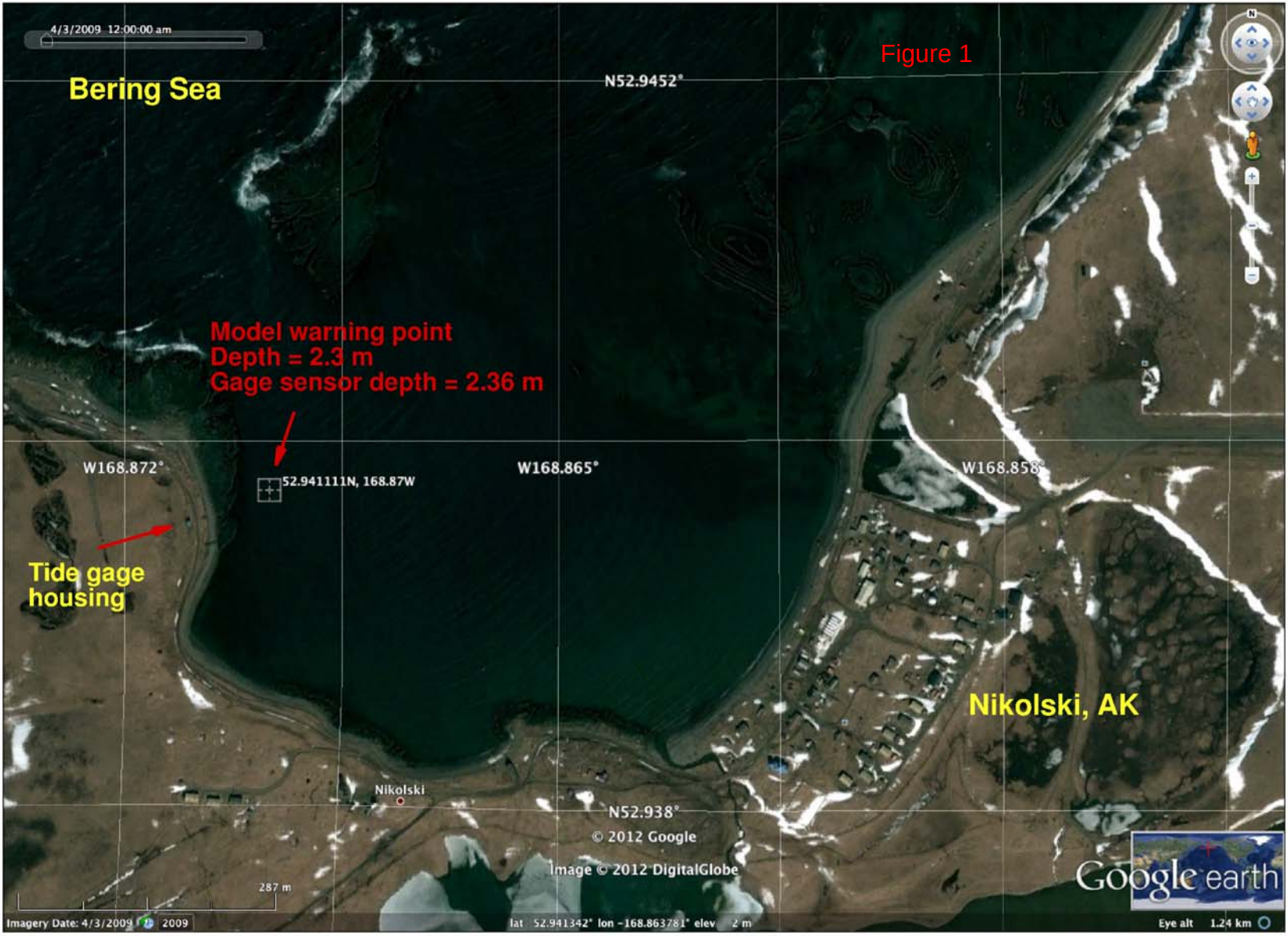
4/3/2009 12:00:00 am
Bering Sea
Figure 1
N52.9452°
Model warning point
Depth = 2.3 m
Gage sensor depth = 2.36 m
W168.872°
52.941111N, 168.87W
W168.865°
W168.858°
Tide gage housing
Nikolski, AK
Nikolski
N52.938°
© 2012 Google
Image © 2012 DigitalGlobe
287 m
Google earth
Imagery Date: 4/3/2009 2009
lat 52.941342° lon -168.863781° elev 2 m
Eye alt 1.24 km

(b)


Tide gage housing
Welcome To
NIKOLSKI
Class of 2004

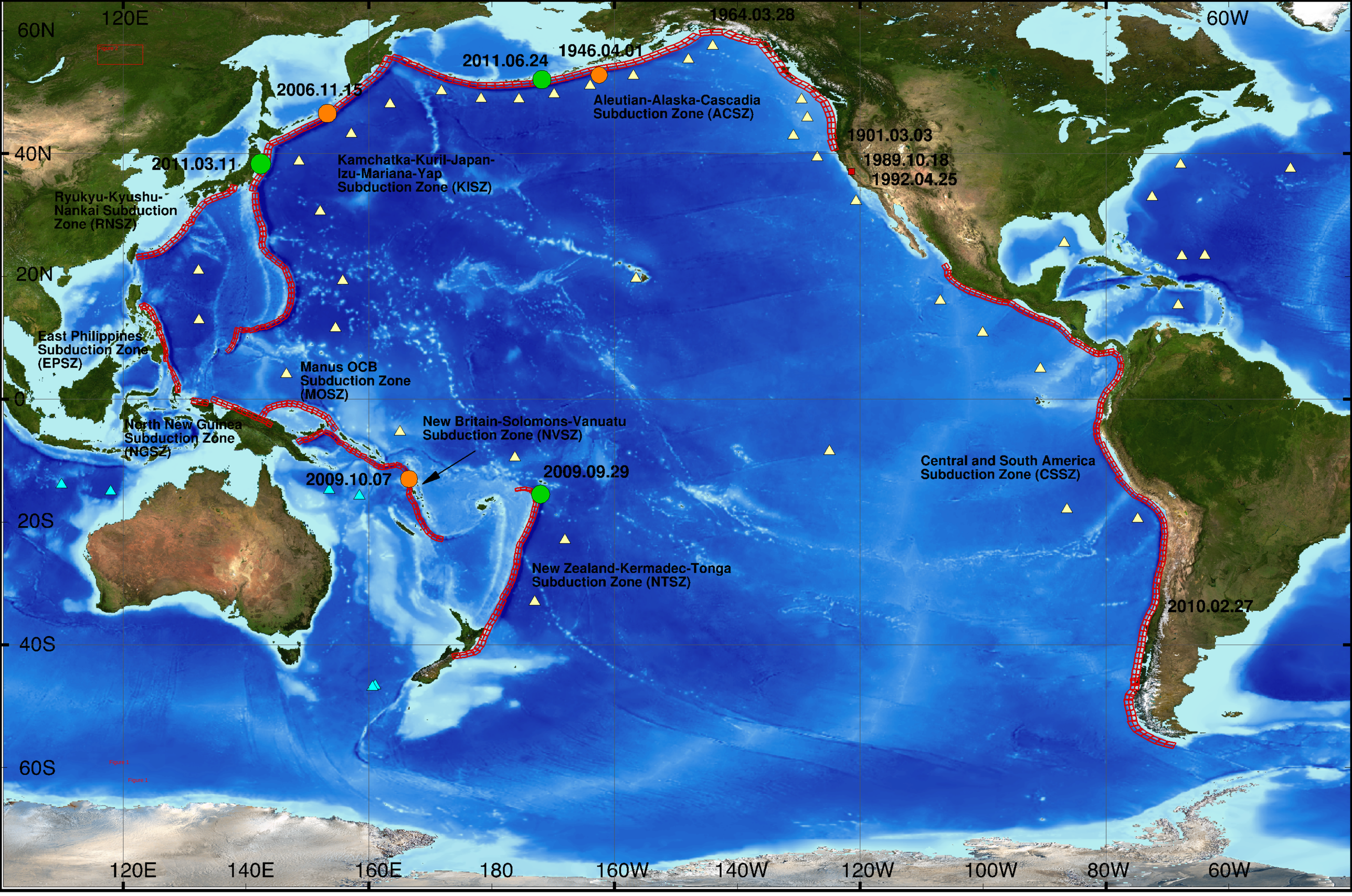
60N
120E
60W
40N
20N
0
20S
40S
60S
120E
140E
160E
180
160W
140W
120W
100W
80W
60W
1964.03.28
1946.04.01
2011.06.24
2006.11.15
2011.03.11
1901.03.03
1989.10.18
1992.04.25
2009.10.07
2009.09.29
2010.02.27
Aleutian-Alaska-Cascadia Subduction Zone (ACSZ)
Kamchatka-Kuril-Japan-Izu-Mariana-Yap Subduction Zone (KISZ)
Ryukyu-Kyushu-Nankai Subduction Zone (RNSZ)
East Philippines Subduction Zone (EPSZ)
Manus OCB Subduction Zone (MOSZ)
North New Guinea Subduction Zone (NGSZ)
New Britain-Solomons-Vanuatu Subduction Zone (NVSZ)
New Zealand-Kermadec-Tonga Subduction Zone (NTSZ)
Central and South America Subduction Zone (CSSZ)

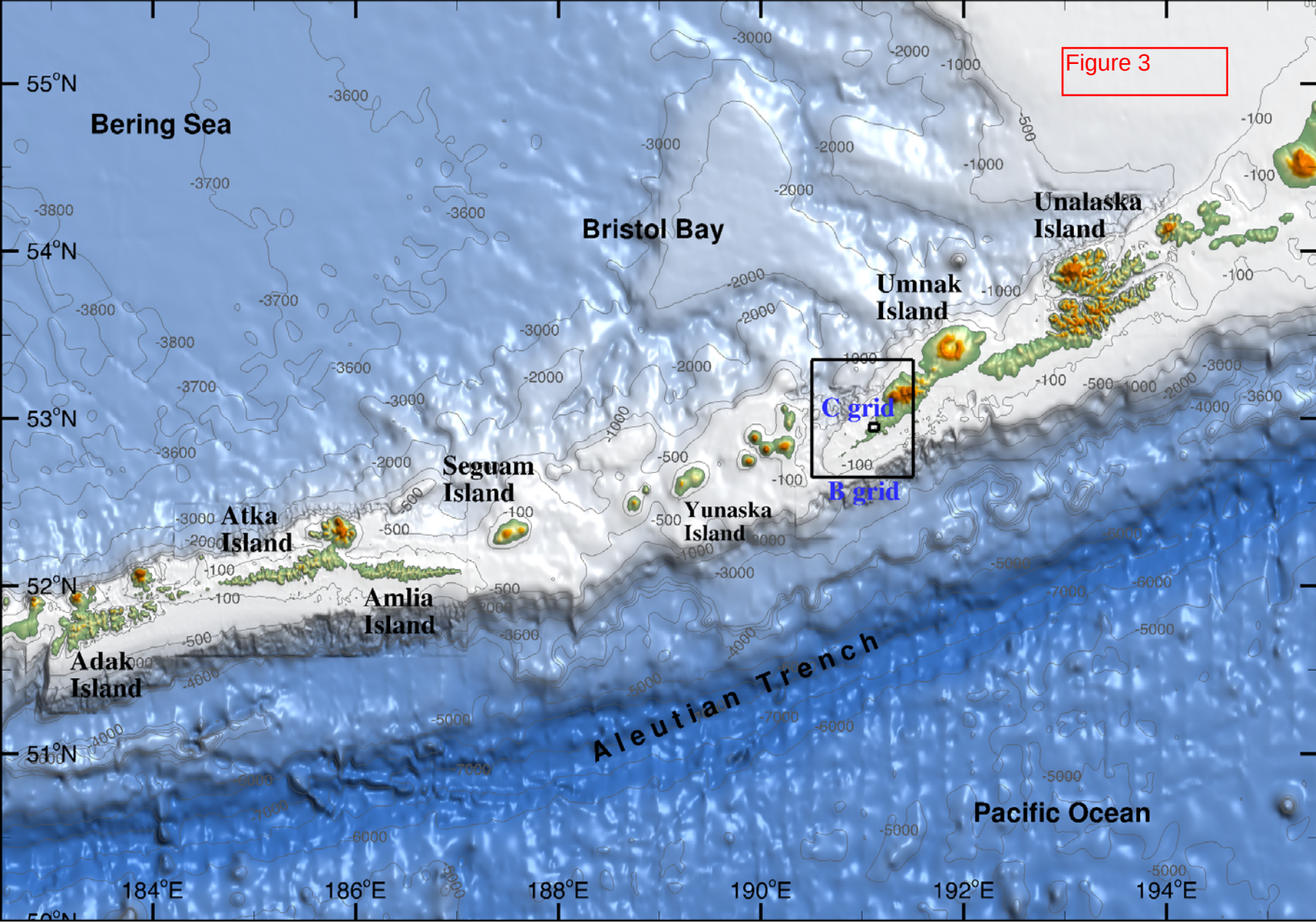
Figure 3
Bering Sea
Bristol Bay
Unalaska Island
Umnak Island
C grid
B grid
Seguam Island
Atka Island
Amlia Island
Yunaska Island
Adak Island
Aleutian Trench
Pacific Ocean
55°N
54°N
53°N
52°N
51°N
184°E
186°E
188°E
190°E
192°E
194°E

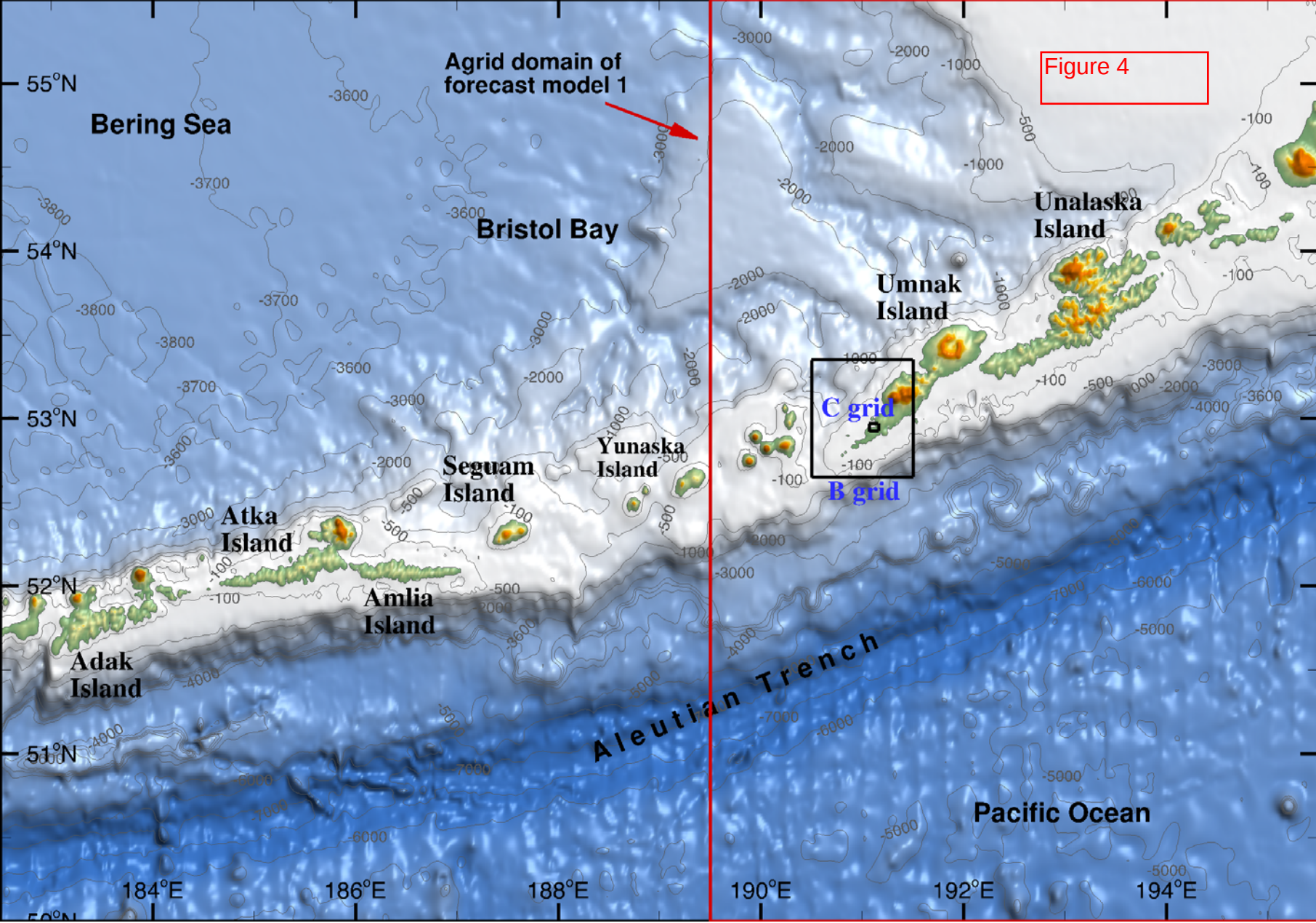
Figure 4
Agrid domain of forecast model 1
Bering Sea
Bristol Bay
Unalaska Island
Umnak Island
C grid
B grid
Yunaska Island
Seguam Island
Atka Island
Amlia Island
Adak Island
Aleutian Trench
Pacific Ocean
55°N
54°N
53°N
52°N
51°N
184°E
186°E
188°E
190°E
192°E
194°E

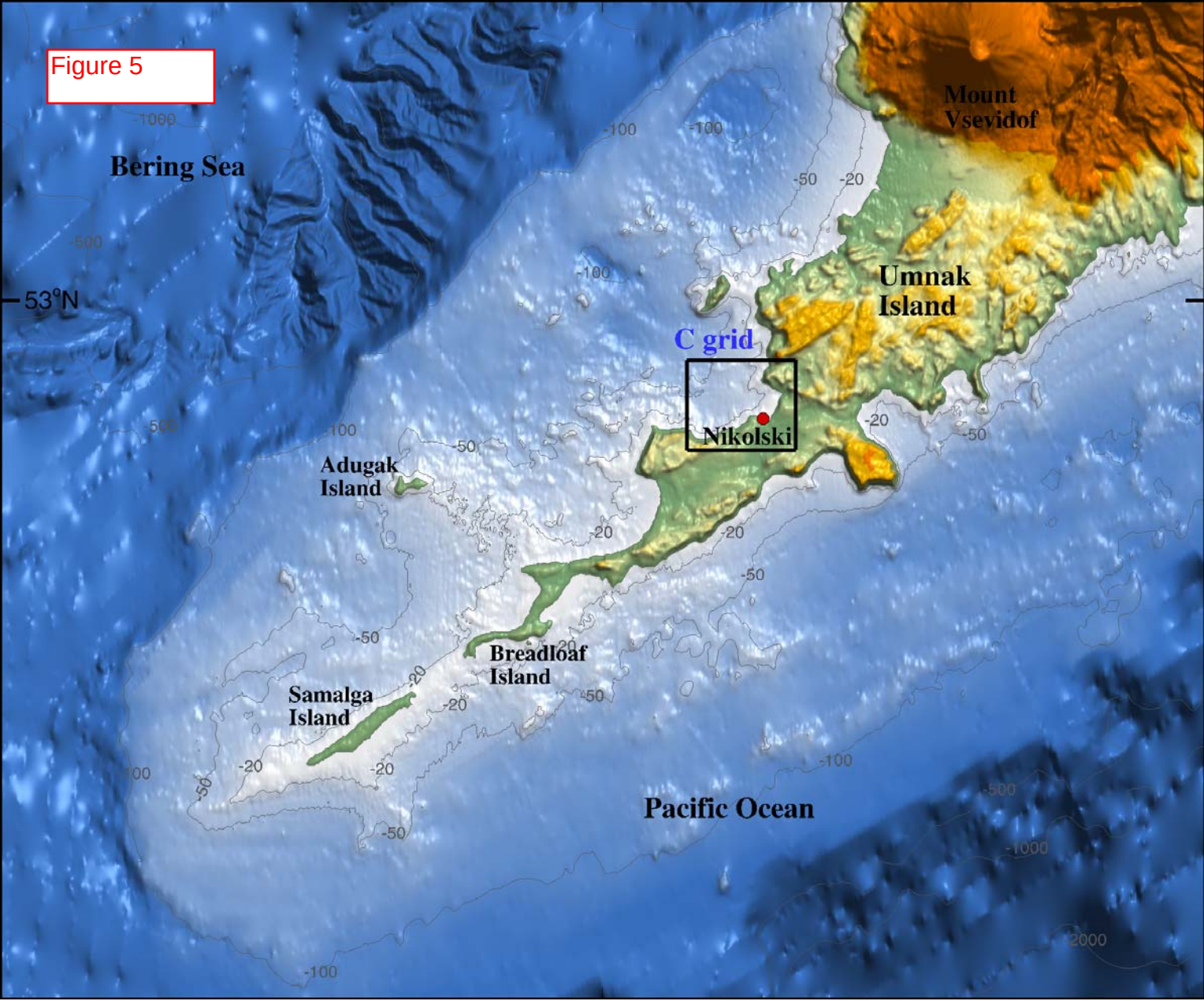
Figure 5
Bering Sea
Mount
Vsevidof
Umnak
Island
C grid
Nikolski
Adugak
Island
Breadloaf
Island
Samalga
Island
Pacific Ocean
53°N

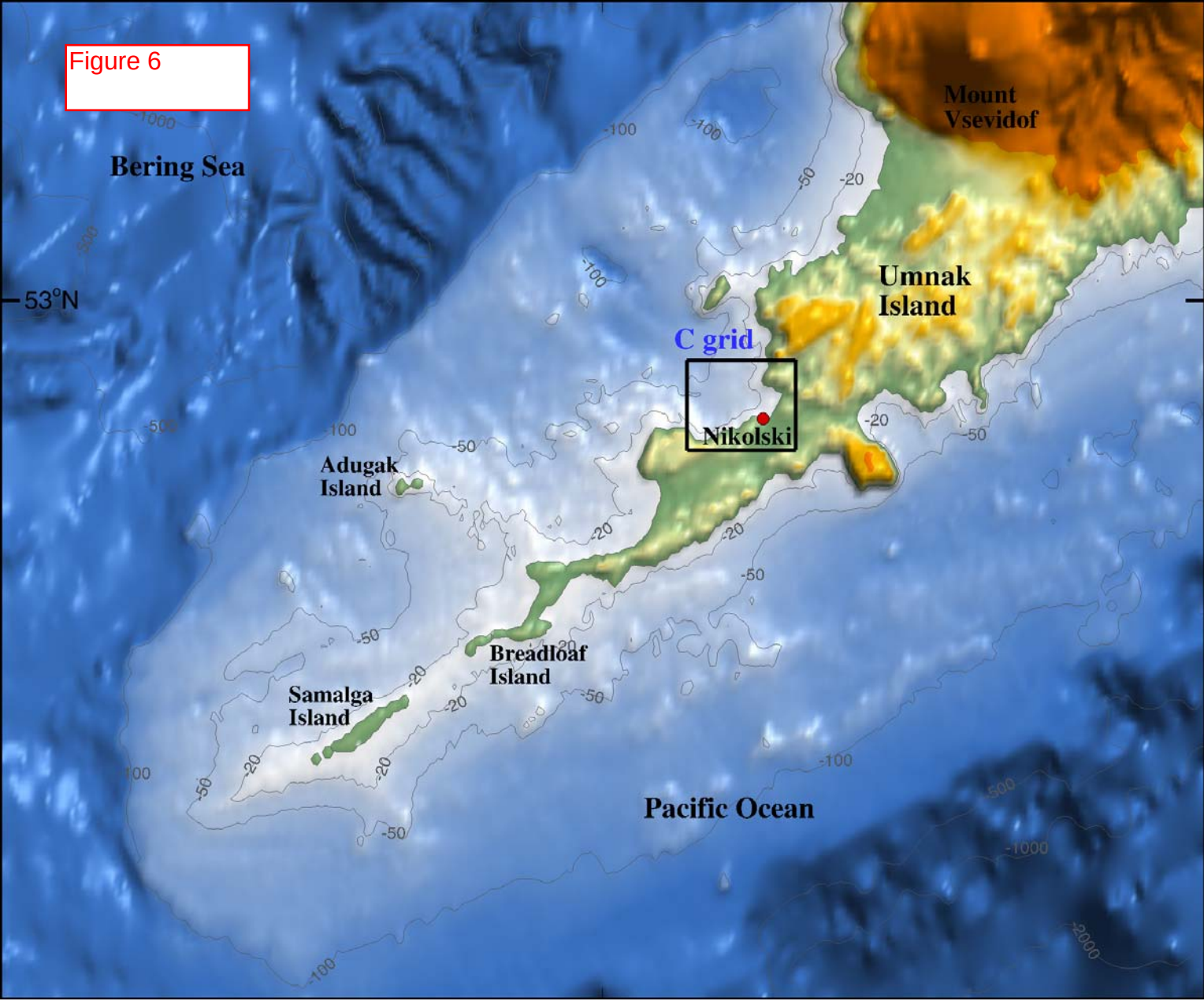
Figure 6
Bering Sea
53°N
Mount
Vsevidof
Umnak
Island
C grid
Nikolski
Adugak
Island
Breadloaf
Island
Samalga
Island
Pacific Ocean
-1000
-500
-100
-50
-20
100
2000

Figure 7

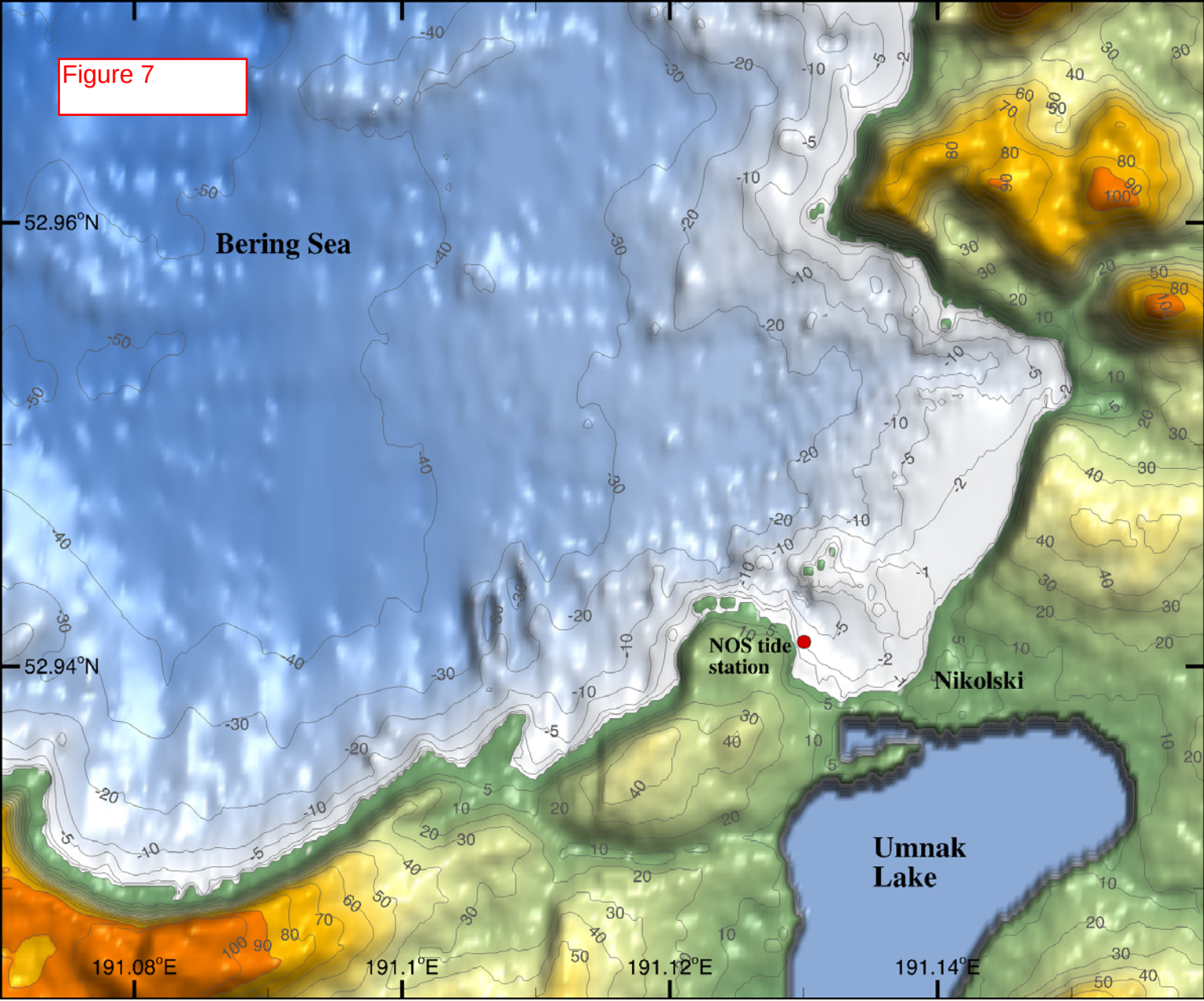
52.96°N
Bering Sea
52.94°N
NOS tide station
Nikolski
Umnak Lake
191.08°E
191.1°E
191.12°E
191.14°E

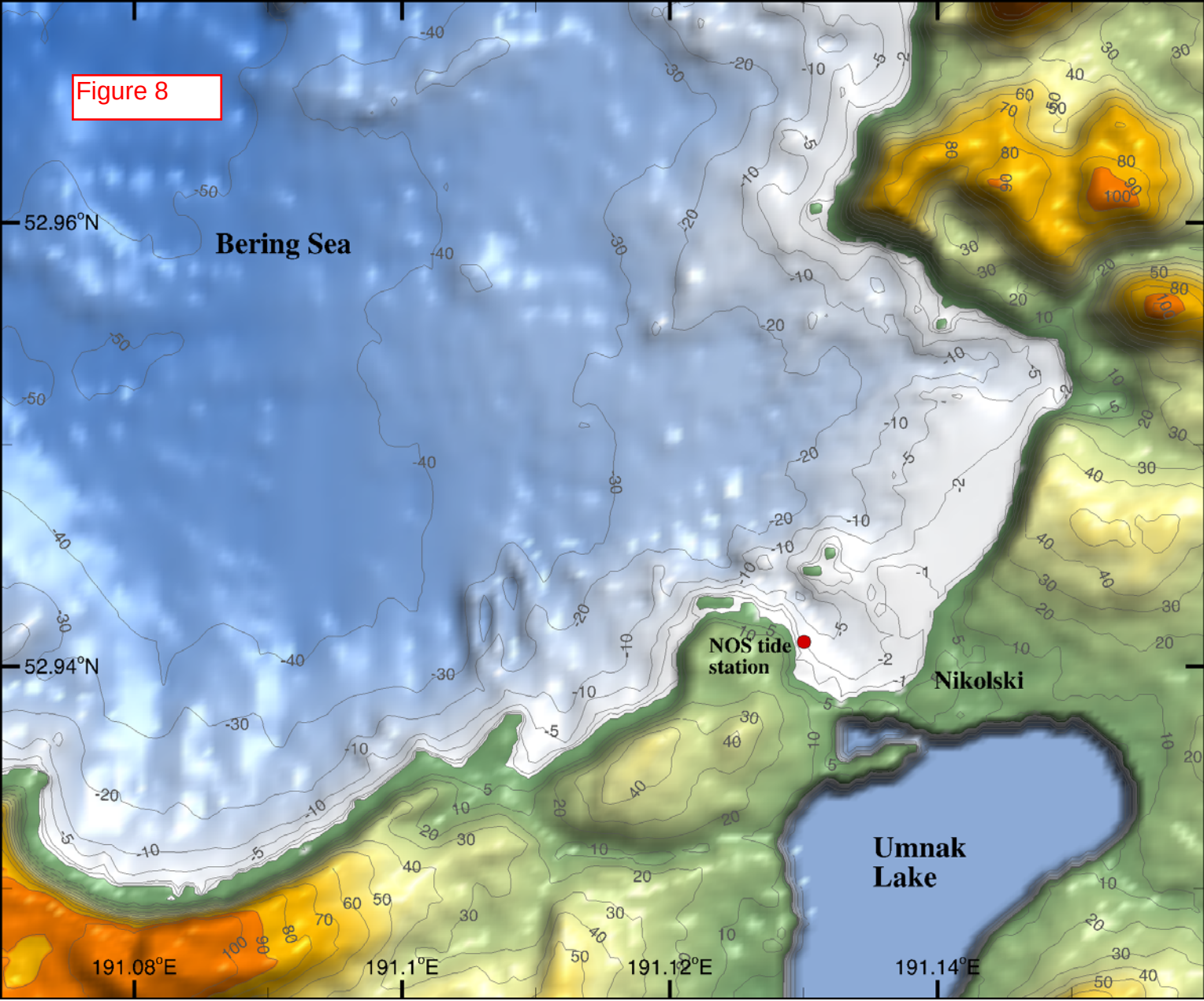
Figure 8
52.96°N
Bering Sea
52.94°N
NOS tide station
Nikolski
Umnak Lake
191.08°E
191.1°E
191.12°E
191.14°E

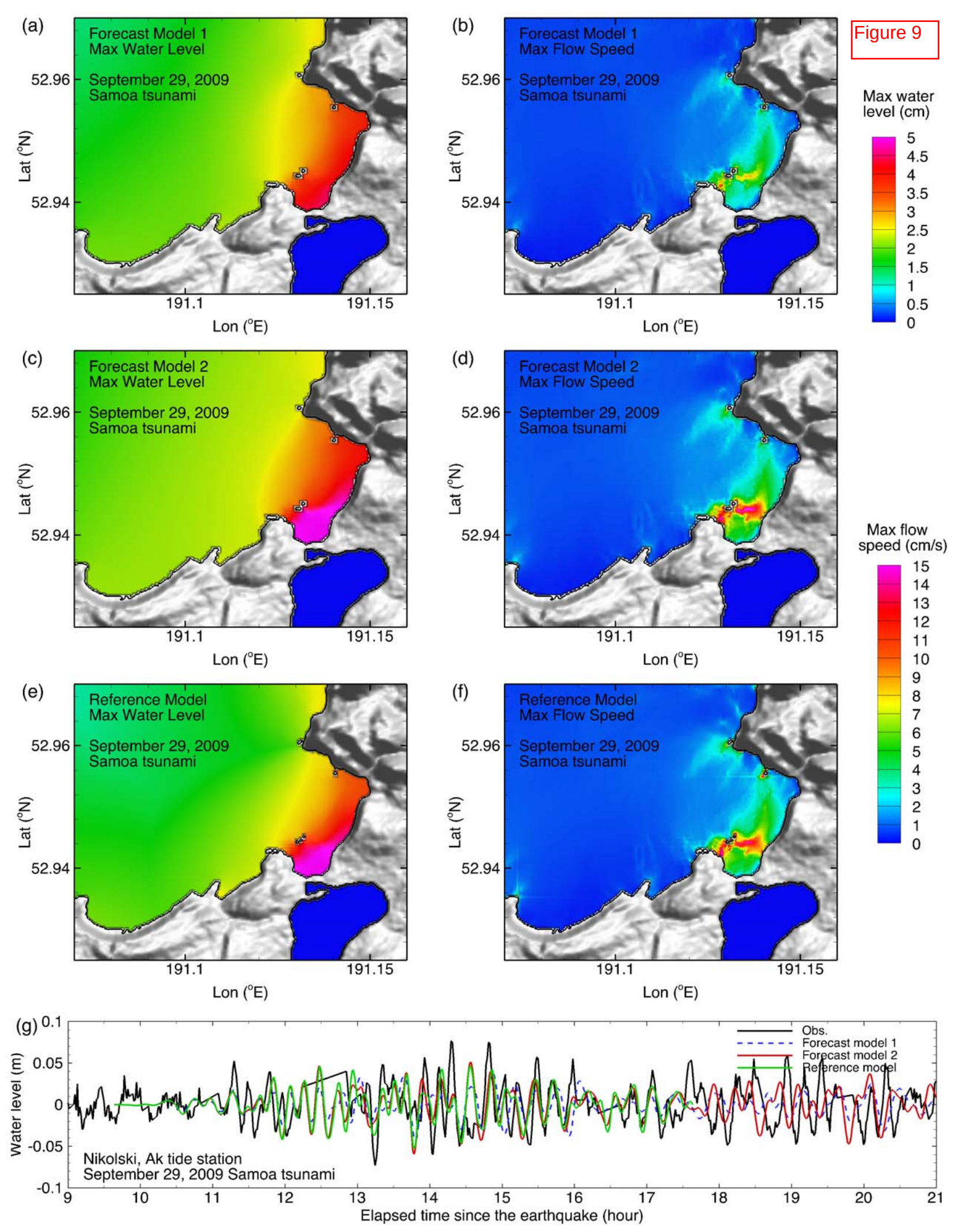
(a)
Forecast Model 1
Max Water Level
September 29, 2009
Samoa tsunami
(b)
Forecast Model 1
Max Flow Speed
September 29, 2009
Samoa tsunami
Max water level (cm)
5
4.5
4
3.5
3
2.5
2
1.5
1
0.5
0
(c)
Forecast Model 2
Max Water Level
September 29, 2009
Samoa tsunami
(d)
Forecast Model 2
Max Flow Speed
September 29, 2009
Samoa tsunami
Max flow speed (cm/s)
15
14
13
12
11
10
9
8
7
6
5
4
3
2
1
0
(e)
Reference Model
Max Water Level
September 29, 2009
Samoa tsunami
(f)
Reference Model
Max Flow Speed
September 29, 2009
Samoa tsunami
52.96
52.94
Lat (°N)
191.1
191.15
Lon (°E)
(g)
Obs.
Forecast model 1
Forecast model 2
Reference model
Nikolski, Ak tide station
September 29, 2009 Samoa tsunami
Water level (m)
0.1
0.05
0
-0.05
-0.1
9
10
11
12
13
14
15
16
17
18
19
20
21
Elapsed time since the earthquake (hour)

Figure 9

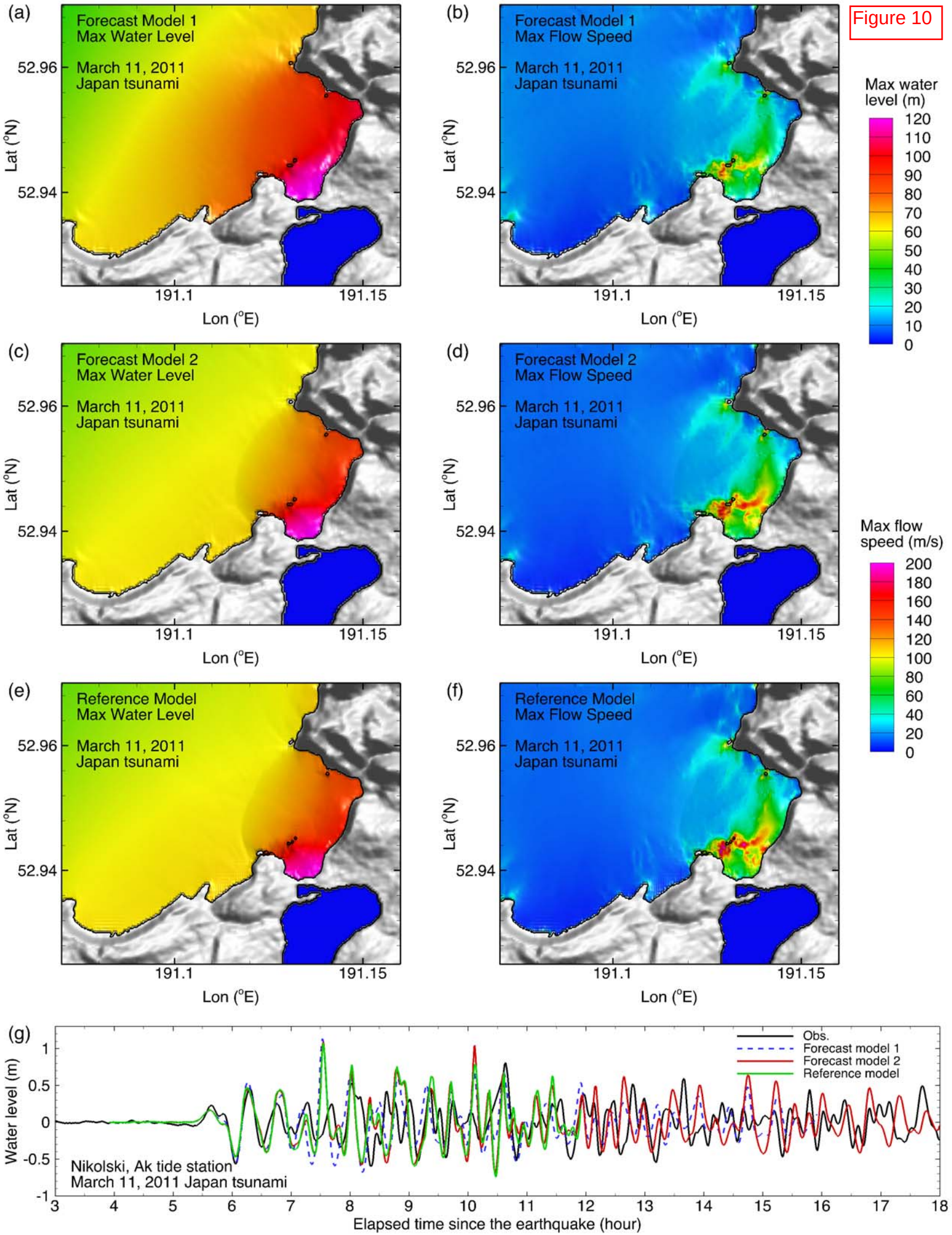
Figure 10
(a)
Forecast Model 1
Max Water Level
March 11, 2011
Japan tsunami
(b)
Forecast Model 1
Max Flow Speed
March 11, 2011
Japan tsunami
Max water level (m)
120
110
100
90
80
70
60
50
40
30
20
10
0
(c)
Forecast Model 2
Max Water Level
March 11, 2011
Japan tsunami
(d)
Forecast Model 2
Max Flow Speed
March 11, 2011
Japan tsunami
Max flow speed (m/s)
200
180
160
140
120
100
80
60
40
20
0
(e)
Reference Model
Max Water Level
March 11, 2011
Japan tsunami
(f)
Reference Model
Max Flow Speed
March 11, 2011
Japan tsunami
52.96
52.94
Lat (°N)
191.1
191.15
Lon (°E)
(g)
Water level (m)
1
0.5
0
-0.5
-1
Nikolski, Ak tide station
March 11, 2011 Japan tsunami
Obs.
Forecast model 1
Forecast model 2
Reference model
3
4
5
6
7
8
9
10
11
12
13
14
15
16
17
18
Elapsed time since the earthquake (hour)

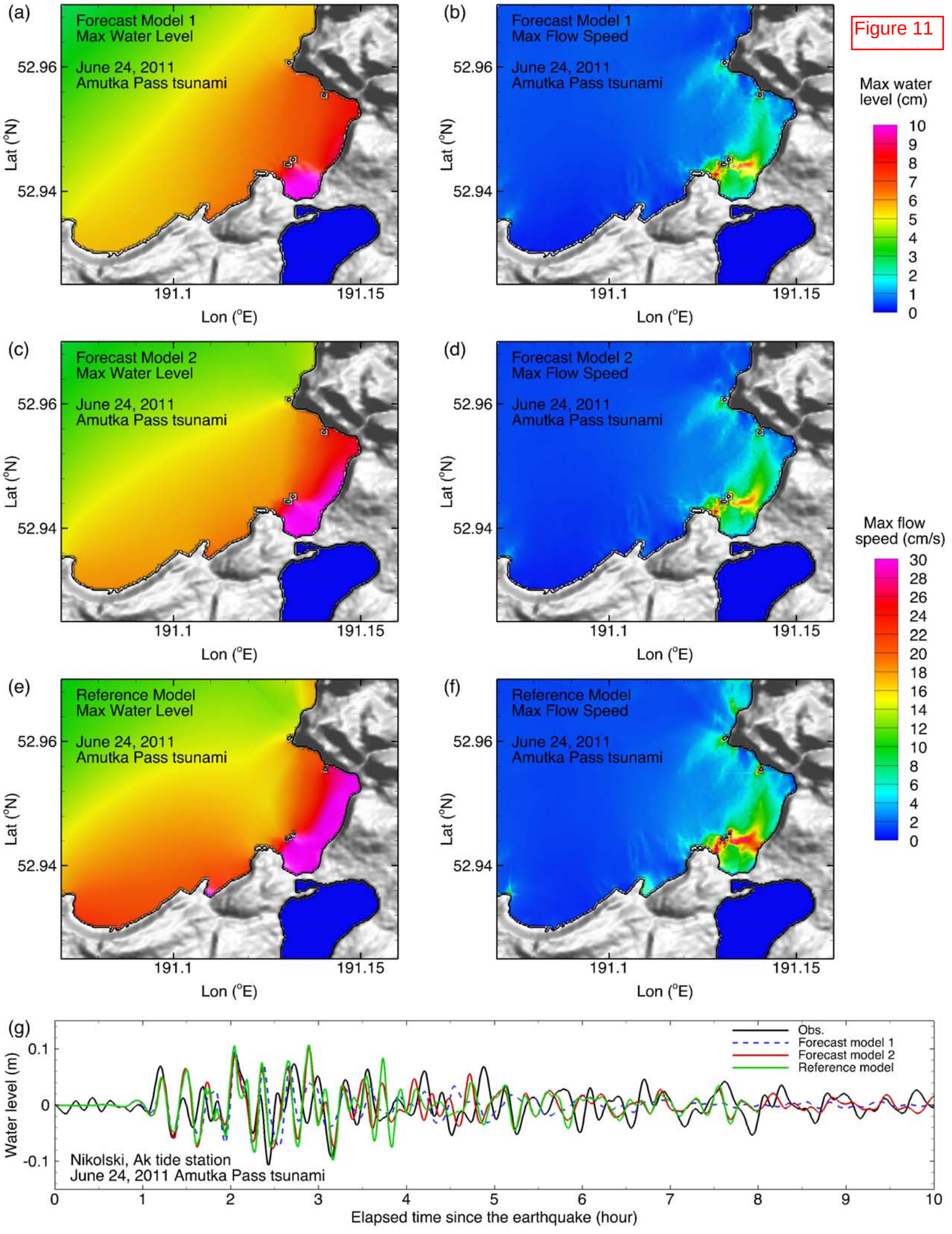
Figure 11
(a)
Forecast Model 1
Max Water Level
June 24, 2011
Amutka Pass tsunami
(b)
Forecast Model 1
Max Flow Speed
June 24, 2011
Amutka Pass tsunami
Max water level (cm)
10
9
8
7
6
5
4
3
2
1
0
(c)
Forecast Model 2
Max Water Level
June 24, 2011
Amutka Pass tsunami
(d)
Forecast Model 2
Max Flow Speed
June 24, 2011
Amutka Pass tsunami
Max flow speed (cm/s)
30
28
26
24
22
20
18
16
14
12
10
8
6
4
2
0
(e)
Reference Model
Max Water Level
June 24, 2011
Amutka Pass tsunami
(f)
Reference Model
Max Flow Speed
June 24, 2011
Amutka Pass tsunami
52.96
52.94
Lat (°N)
191.1
191.15
Lon (°E)
(g)
Water level (m)
0.1
0
-0.1
Nikolski, Ak tide station
June 24, 2011 Amutka Pass tsunami
Obs.
Forecast model 1
Forecast model 2
Reference model
0
1
2
3
4
5
6
7
8
9
10
Elapsed time since the earthquake (hour)

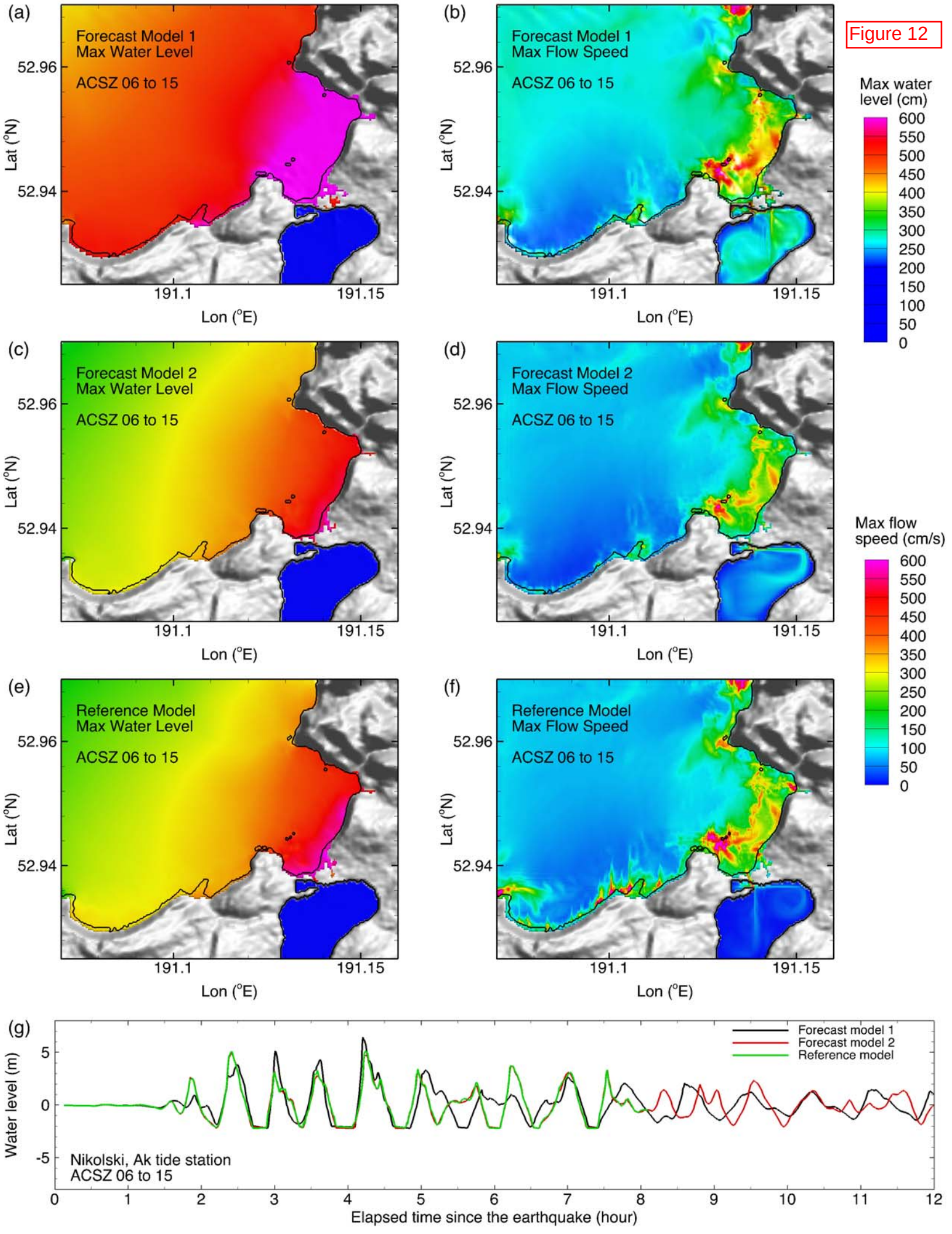
Figure 12
(a)
Forecast Model 1
Max Water Level
ACSZ 06 to 15
(b)
Forecast Model 1
Max Flow Speed
ACSZ 06 to 15
(c)
Forecast Model 2
Max Water Level
ACSZ 06 to 15
(d)
Forecast Model 2
Max Flow Speed
ACSZ 06 to 15
(e)
Reference Model
Max Water Level
ACSZ 06 to 15
(f)
Reference Model
Max Flow Speed
ACSZ 06 to 15
Lat (°N)
52.96
52.94
Lon (°E)
191.1
191.15
Max water level (cm)
600
550
500
450
400
350
300
250
200
150
100
50
0
Max flow speed (cm/s)
600
550
500
450
400
350
300
250
200
150
100
50
0
(g)
Water level (m)
5
0
-5
Nikolski, Ak tide station
ACSZ 06 to 15
Forecast model 1
Forecast model 2
Reference model
0
1
2
3
4
5
6
7
8
9
10
11
12
Elapsed time since the earthquake (hour)

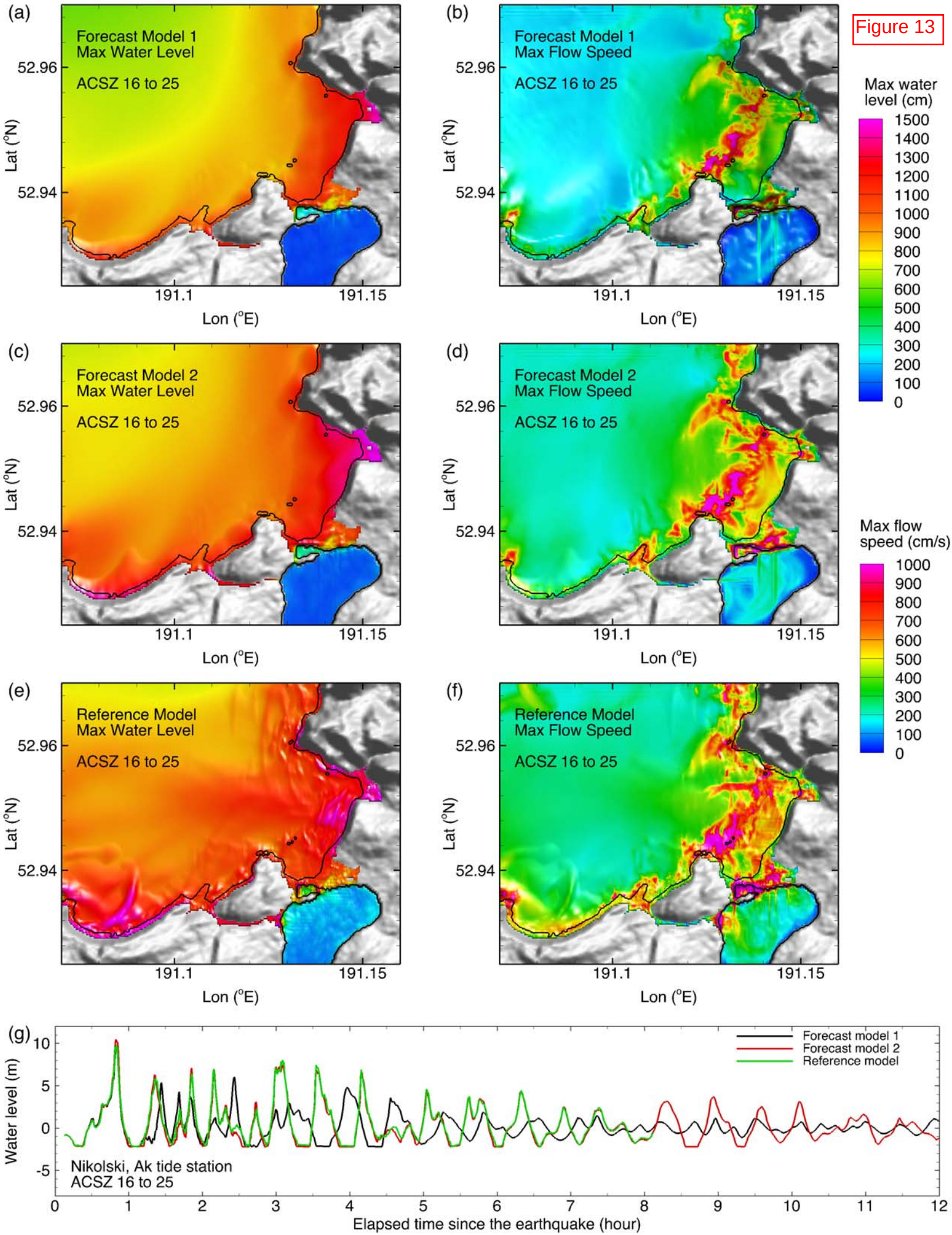
Figure 13
(a)
Forecast Model 1
Max Water Level
ACSZ 16 to 25
(b)
Forecast Model 1
Max Flow Speed
ACSZ 16 to 25
(c)
Forecast Model 2
Max Water Level
ACSZ 16 to 25
(d)
Forecast Model 2
Max Flow Speed
ACSZ 16 to 25
(e)
Reference Model
Max Water Level
ACSZ 16 to 25
(f)
Reference Model
Max Flow Speed
ACSZ 16 to 25
Lat (°N)
52.96
52.94
Lon (°E)
191.1
191.15
Max water level (cm)
1500
1400
1300
1200
1100
1000
900
800
700
600
500
400
300
200
100
0
Max flow speed (cm/s)
1000
900
800
700
600
500
400
300
200
100
0
(g)
Water level (m)
10
5
0
-5
Nikolski, Ak tide station
ACSZ 16 to 25
Forecast model 1
Forecast model 2
Reference model
0
1
2
3
4
5
6
7
8
9
10
11
12
Elapsed time since the earthquake (hour)

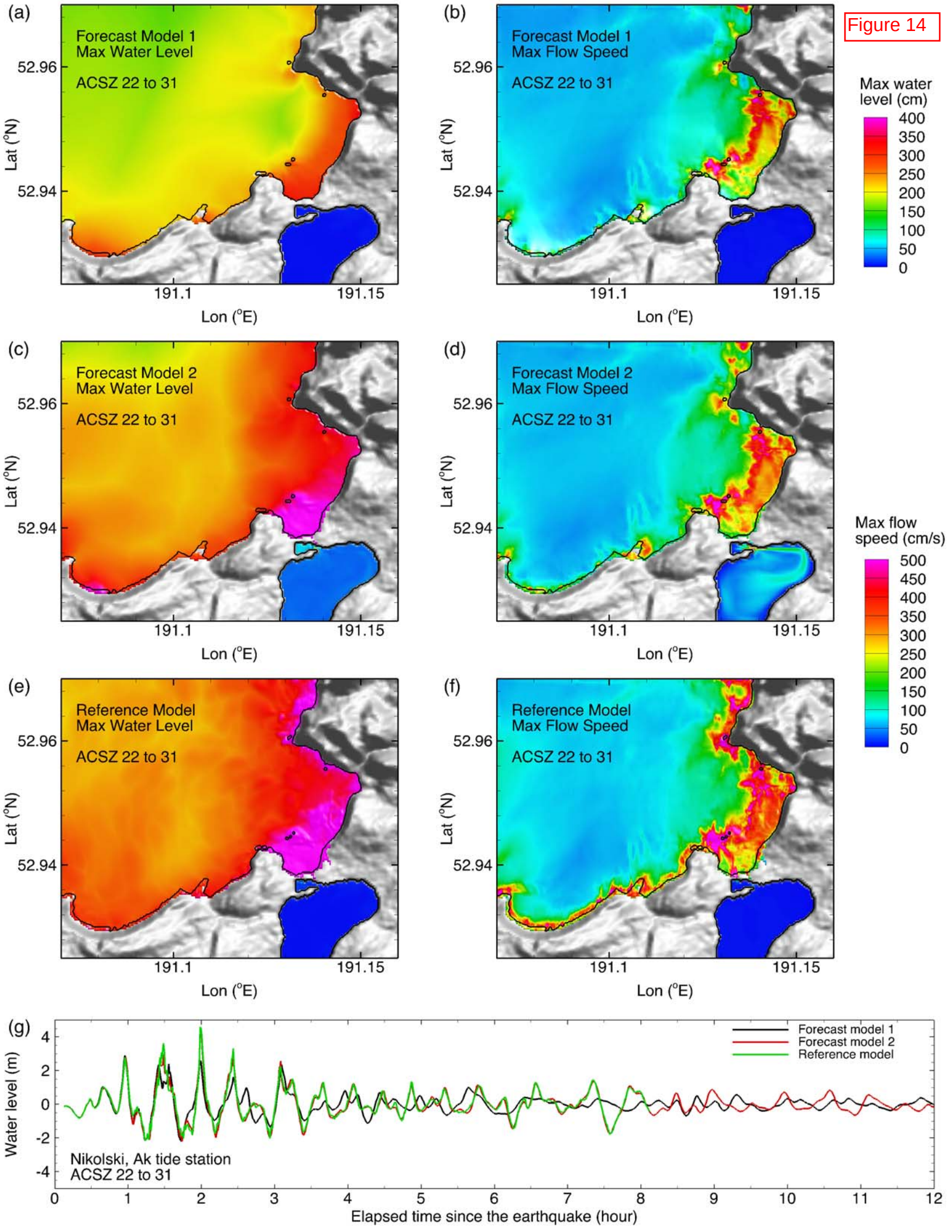
Figure 14
(a)
Forecast Model 1
Max Water Level
ACSZ 22 to 31
(b)
Forecast Model 1
Max Flow Speed
ACSZ 22 to 31
Max water level (cm)
400
350
300
250
200
150
100
50
0
(c)
Forecast Model 2
Max Water Level
ACSZ 22 to 31
(d)
Forecast Model 2
Max Flow Speed
ACSZ 22 to 31
Max flow speed (cm/s)
500
450
400
350
300
250
200
150
100
50
0
(e)
Reference Model
Max Water Level
ACSZ 22 to 31
(f)
Reference Model
Max Flow Speed
ACSZ 22 to 31
Lat (°N)
52.96
52.94
Lon (°E)
191.1
191.15
(g)
Water level (m)
4
2
0
-2
-4
Nikolski, Ak tide station
ACSZ 22 to 31
Forecast model 1
Forecast model 2
Reference model
0
1
2
3
4
5
6
7
8
9
10
11
12
Elapsed time since the earthquake (hour)

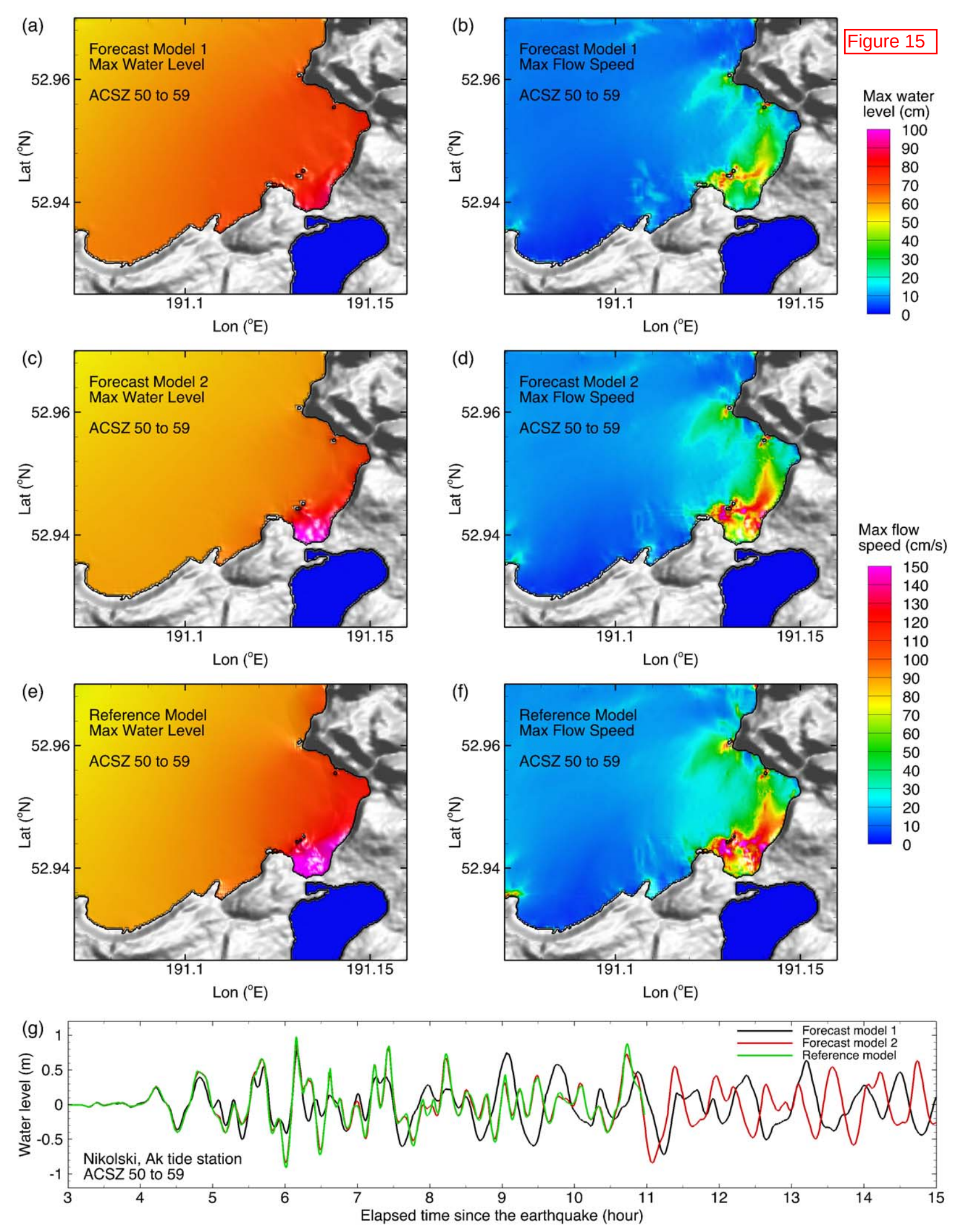
Figure 15
(a)
Forecast Model 1
Max Water Level
ACSZ 50 to 59
(b)
Forecast Model 1
Max Flow Speed
ACSZ 50 to 59
Max water level (cm)
100
90
80
70
60
50
40
30
20
10
0
(c)
Forecast Model 2
Max Water Level
ACSZ 50 to 59
(d)
Forecast Model 2
Max Flow Speed
ACSZ 50 to 59
Max flow speed (cm/s)
150
140
130
120
110
100
90
80
70
60
50
40
30
20
10
0
(e)
Reference Model
Max Water Level
ACSZ 50 to 59
(f)
Reference Model
Max Flow Speed
ACSZ 50 to 59
52.96
52.94
Lat (°N)
191.1
191.15
Lon (°E)
(g)
Forecast model 1
Forecast model 2
Reference model
Water level (m)
1
0.5
0
-0.5
-1
Nikolski, Ak tide station
ACSZ 50 to 59
3
4
5
6
7
8
9
10
11
12
13
14
15
Elapsed time since the earthquake (hour)

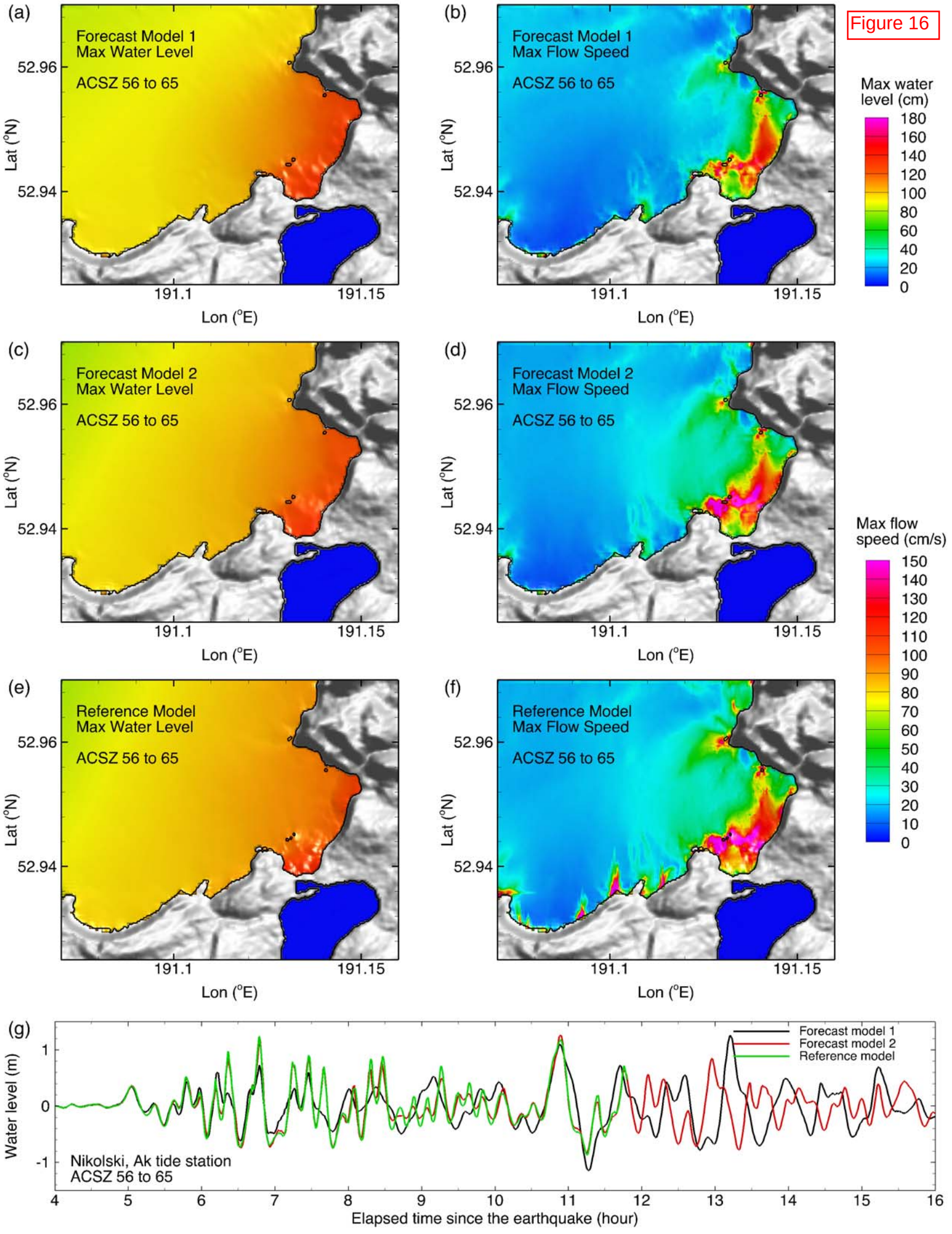
Figure 16
(a)
Forecast Model 1
Max Water Level
ACSZ 56 to 65
(b)
Forecast Model 1
Max Flow Speed
ACSZ 56 to 65
Max water level (cm)
180
160
140
120
100
80
60
40
20
0
(c)
Forecast Model 2
Max Water Level
ACSZ 56 to 65
(d)
Forecast Model 2
Max Flow Speed
ACSZ 56 to 65
Max flow speed (cm/s)
150
140
130
120
110
100
90
80
70
60
50
40
30
20
10
0
(e)
Reference Model
Max Water Level
ACSZ 56 to 65
(f)
Reference Model
Max Flow Speed
ACSZ 56 to 65
52.96
52.94
Lat (°N)
191.1
191.15
Lon (°E)
(g)
Water level (m)
1
0
-1
Nikolski, Ak tide station
ACSZ 56 to 65
Forecast model 1
Forecast model 2
Reference model
4
5
6
7
8
9
10
11
12
13
14
15
16
Elapsed time since the earthquake (hour)

Figure 17

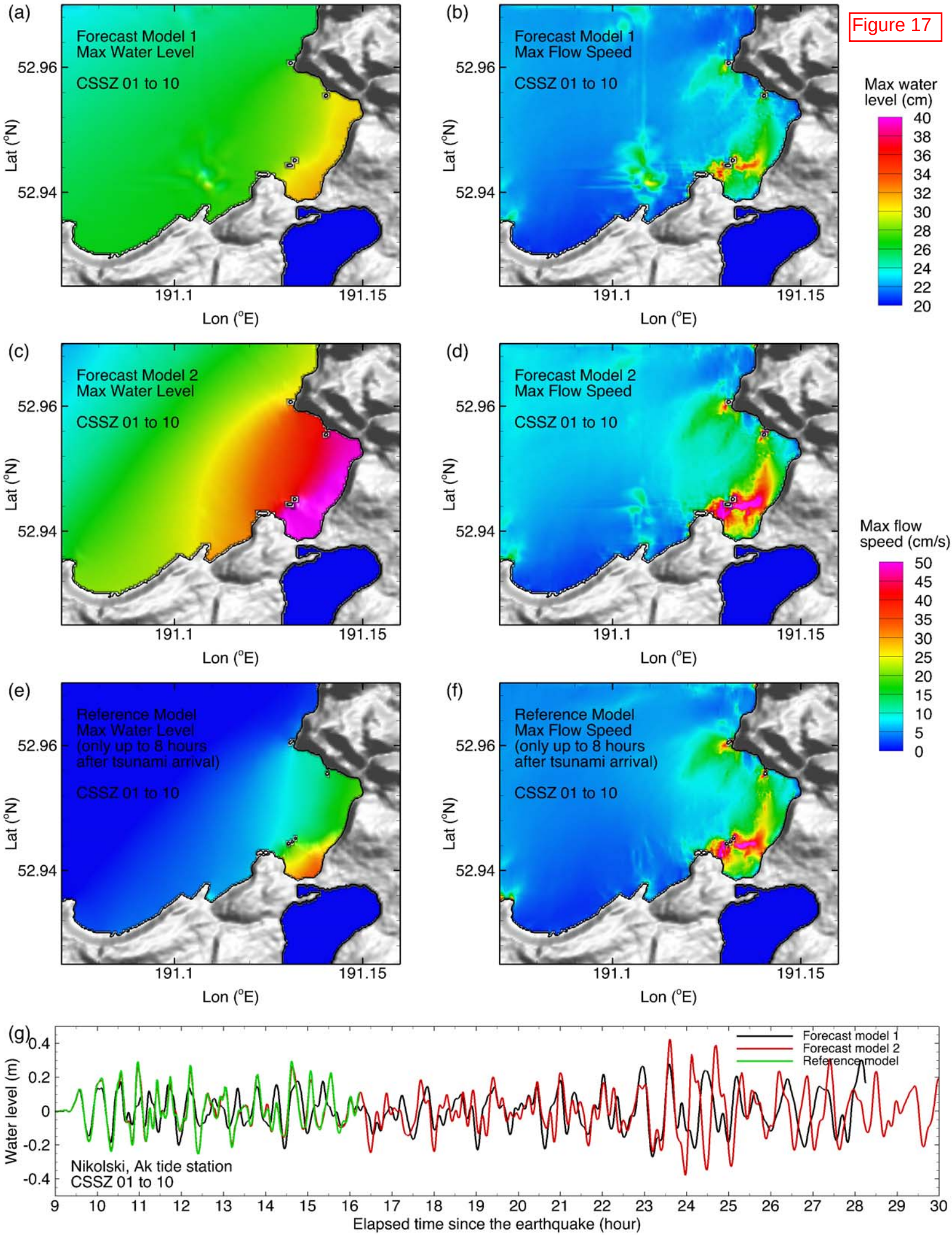
(a)
Forecast Model 1
Max Water Level
CSSZ 01 to 10
(b)
Forecast Model 1
Max Flow Speed
CSSZ 01 to 10
Max water level (cm)
40
38
36
34
32
30
28
26
24
22
20
(c)
Forecast Model 2
Max Water Level
CSSZ 01 to 10
(d)
Forecast Model 2
Max Flow Speed
CSSZ 01 to 10
Max flow speed (cm/s)
50
45
40
35
30
25
20
15
10
5
0
(e)
Reference Model
Max Water Level
(only up to 8 hours
after tsunami arrival)
CSSZ 01 to 10
(f)
Reference Model
Max Flow Speed
(only up to 8 hours
after tsunami arrival)
CSSZ 01 to 10
Lat (°N)
52.96
52.94
Lon (°E)
191.1
191.15
(g)
Water level (m)
0.4
0.2
0
-0.2
-0.4
Nikolski, Ak tide station
CSSZ 01 to 10
Forecast model 1
Forecast model 2
Reference model
9
10
11
12
13
14
15
16
17
18
19
20
21
22
23
24
25
26
27
28
29
30
Elapsed time since the earthquake (hour)

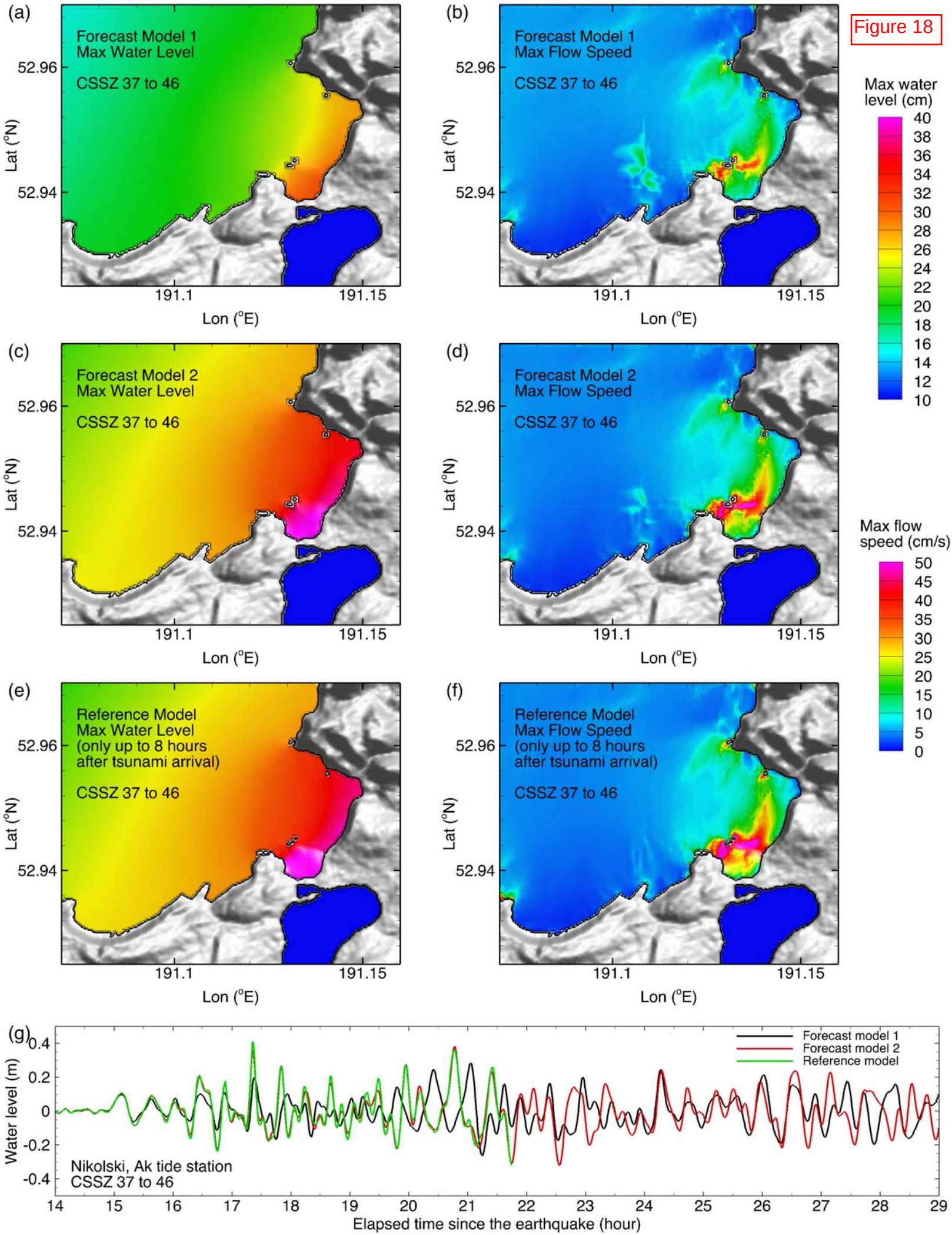
Figure 18
(a)
Forecast Model 1
Max Water Level
CSSZ 37 to 46
(b)
Forecast Model 1
Max Flow Speed
CSSZ 37 to 46
(c)
Forecast Model 2
Max Water Level
CSSZ 37 to 46
(d)
Forecast Model 2
Max Flow Speed
CSSZ 37 to 46
(e)
Reference Model
Max Water Level
(only up to 8 hours
after tsunami arrival)
CSSZ 37 to 46
(f)
Reference Model
Max Flow Speed
(only up to 8 hours
after tsunami arrival)
CSSZ 37 to 46
Lat (°N)
52.96
52.94
Lon (°E)
191.1
191.15
Max water level (cm)
40
38
36
34
32
30
28
26
24
22
20
18
16
14
12
10
Max flow speed (cm/s)
50
45
40
35
30
25
20
15
10
5
0
(g)
Water level (m)
0.4
0.2
0
-0.2
-0.4
Nikolski, Ak tide station
CSSZ 37 to 46
Forecast model 1
Forecast model 2
Reference model
14
15
16
17
18
19
20
21
22
23
24
25
26
27
28
29
Elapsed time since the earthquake (hour)

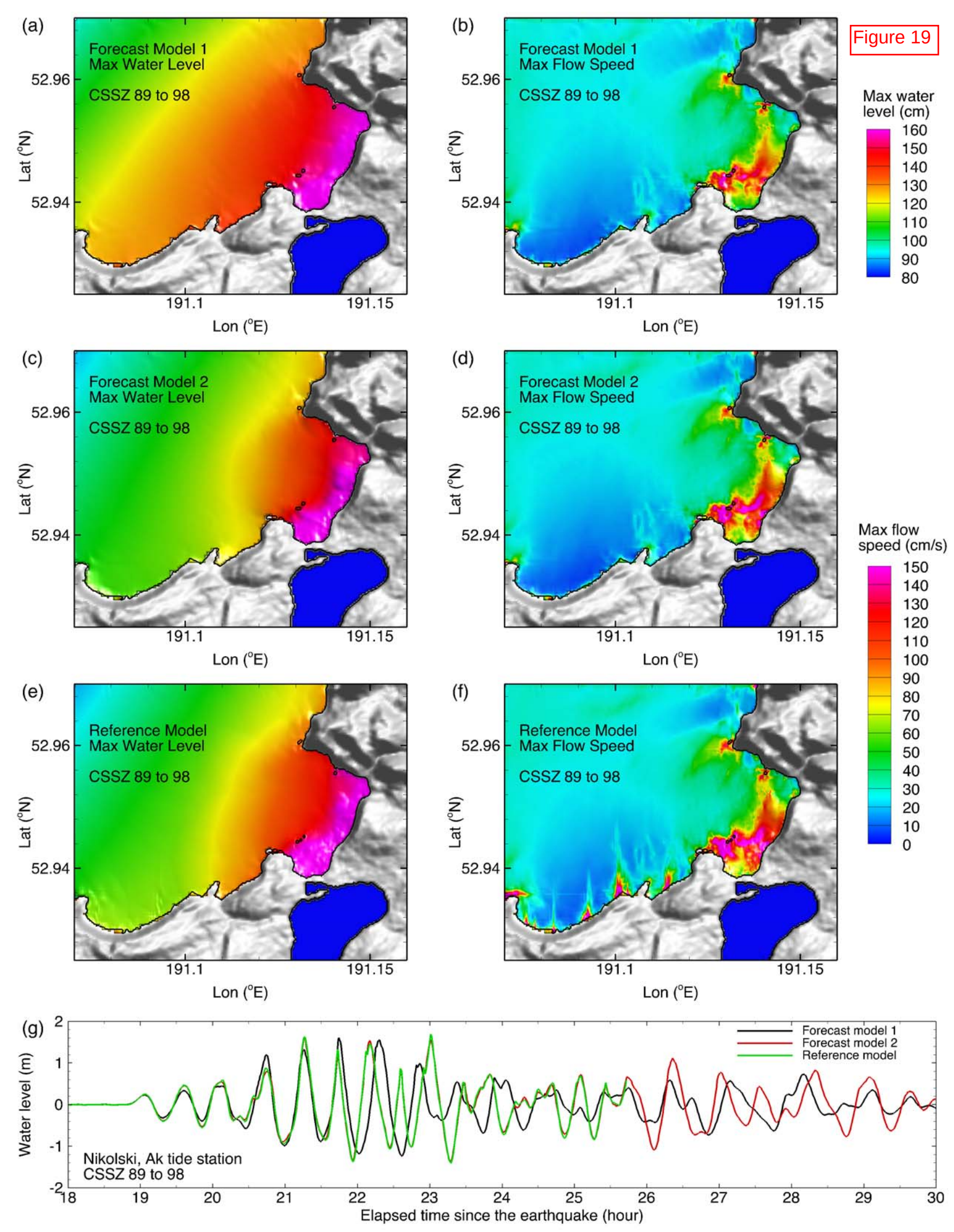
Figure 19
(a)
Forecast Model 1
Max Water Level
CSSZ 89 to 98
(b)
Forecast Model 1
Max Flow Speed
CSSZ 89 to 98
Max water level (cm)
160
150
140
130
120
110
100
90
80
(c)
Forecast Model 2
Max Water Level
CSSZ 89 to 98
(d)
Forecast Model 2
Max Flow Speed
CSSZ 89 to 98
Max flow speed (cm/s)
150
140
130
120
110
100
90
80
70
60
50
40
30
20
10
0
(e)
Reference Model
Max Water Level
CSSZ 89 to 98
(f)
Reference Model
Max Flow Speed
CSSZ 89 to 98
52.96
52.94
Lat (°N)
191.1
191.15
Lon (°E)
(g)
Water level (m)
2
1
0
-1
-2
Nikolski, Ak tide station
CSSZ 89 to 98
Forecast model 1
Forecast model 2
Reference model
18
19
20
21
22
23
24
25
26
27
28
29
30
Elapsed time since the earthquake (hour)

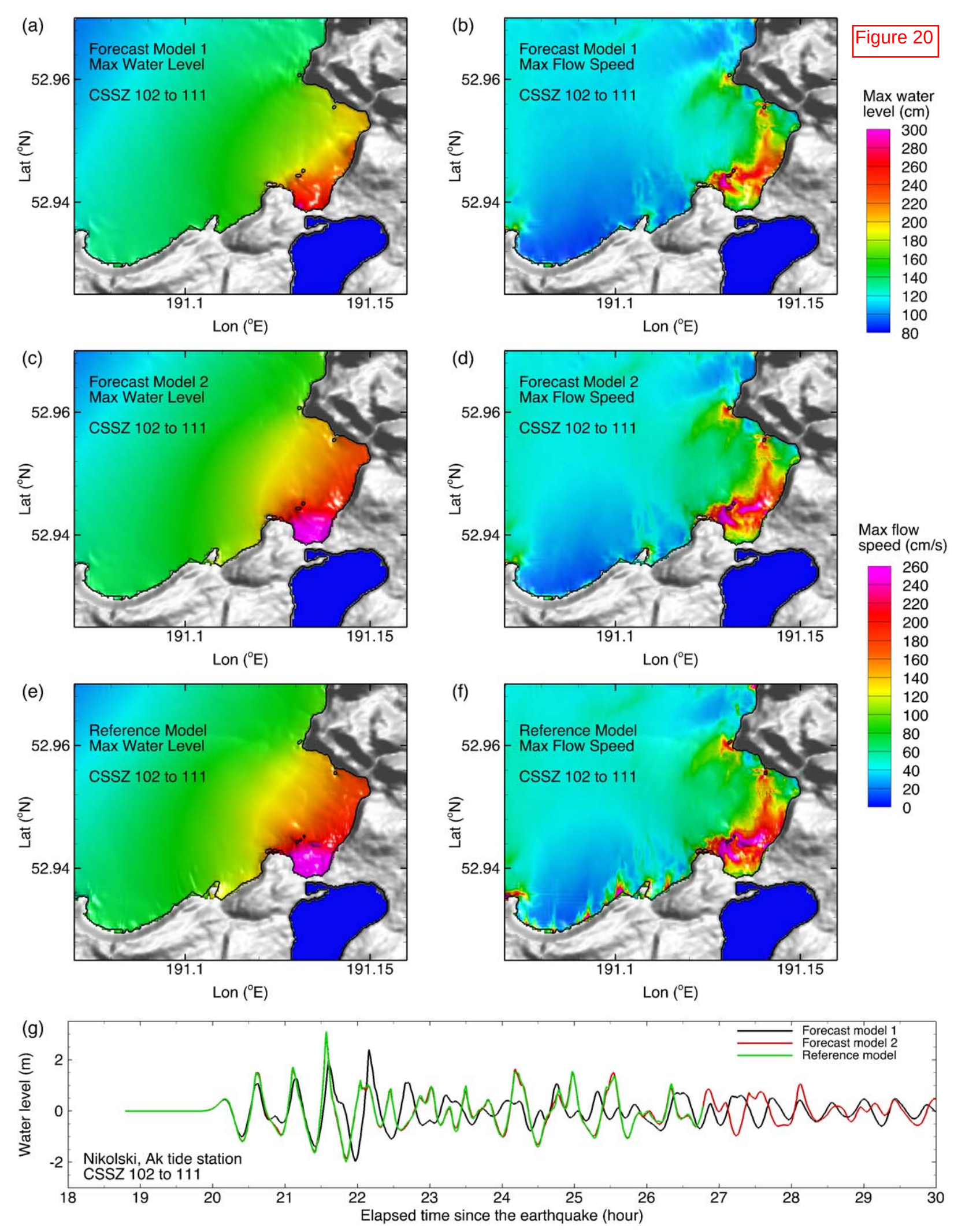
Figure 20
(a)
Forecast Model 1
Max Water Level
CSSZ 102 to 111
(b)
Forecast Model 1
Max Flow Speed
CSSZ 102 to 111
Max water level (cm)
300
280
260
240
220
200
180
160
140
120
100
80
(c)
Forecast Model 2
Max Water Level
CSSZ 102 to 111
(d)
Forecast Model 2
Max Flow Speed
CSSZ 102 to 111
Max flow speed (cm/s)
260
240
220
200
180
160
140
120
100
80
60
40
20
0
(e)
Reference Model
Max Water Level
CSSZ 102 to 111
(f)
Reference Model
Max Flow Speed
CSSZ 102 to 111
52.96
52.94
Lat (°N)
191.1
191.15
Lon (°E)
(g)
Forecast model 1
Forecast model 2
Reference model
Water level (m)
2
0
-2
Nikolski, Ak tide station
CSSZ 102 to 111
18
19
20
21
22
23
24
25
26
27
28
29
30
Elapsed time since the earthquake (hour)

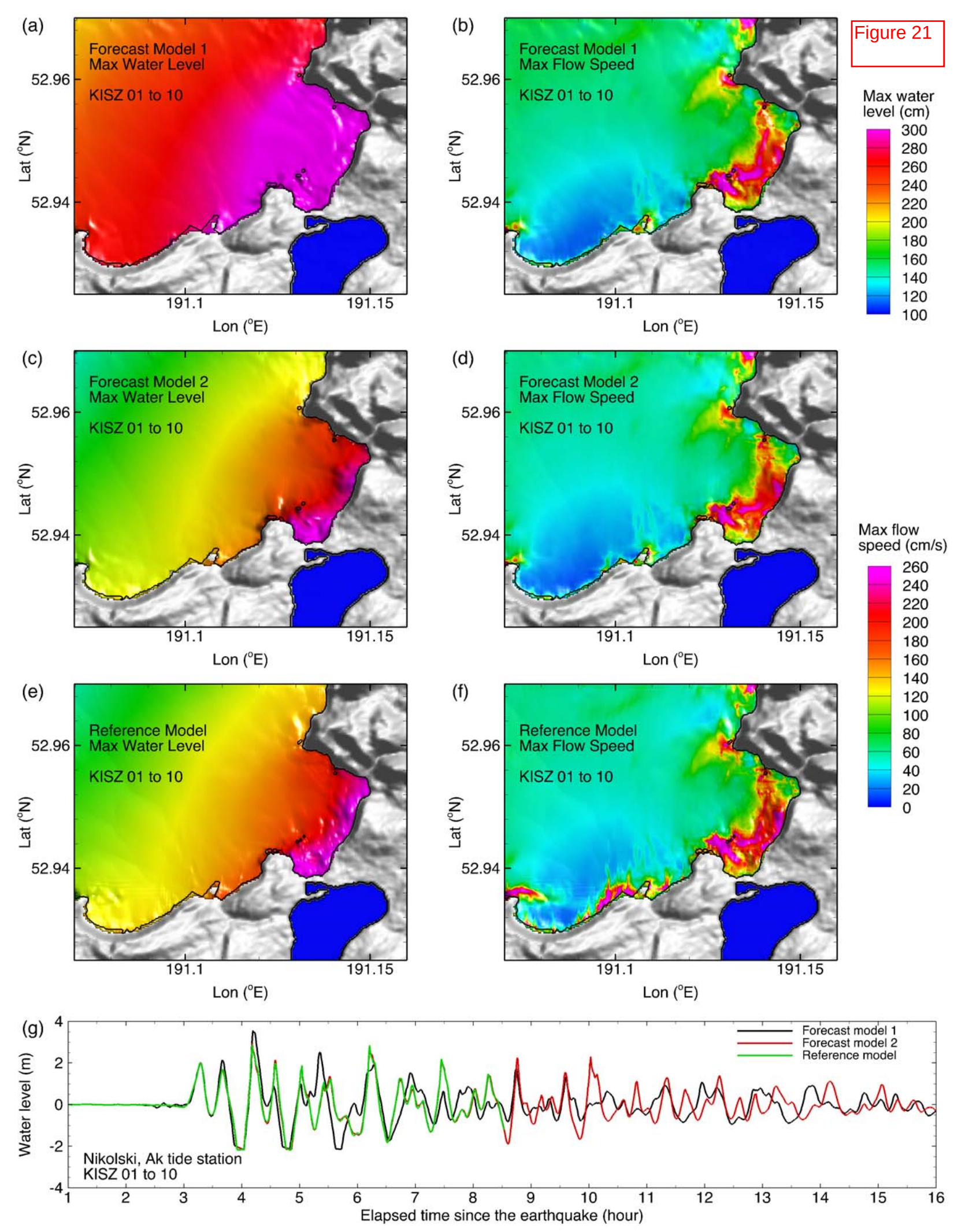
Figure 21
(a)
Forecast Model 1
Max Water Level
KISZ 01 to 10
(b)
Forecast Model 1
Max Flow Speed
KISZ 01 to 10
Max water level (cm)
300
280
260
240
220
200
180
160
140
120
100
(c)
Forecast Model 2
Max Water Level
KISZ 01 to 10
(d)
Forecast Model 2
Max Flow Speed
KISZ 01 to 10
Max flow speed (cm/s)
260
240
220
200
180
160
140
120
100
80
60
40
20
0
(e)
Reference Model
Max Water Level
KISZ 01 to 10
(f)
Reference Model
Max Flow Speed
KISZ 01 to 10
52.96
52.94
Lat (°N)
191.1
191.15
Lon (°E)
(g)
Forecast model 1
Forecast model 2
Reference model
Water level (m)
4
2
0
-2
-4
Nikolski, Ak tide station
KISZ 01 to 10
1
2
3
4
5
6
7
8
9
10
11
12
13
14
15
16
Elapsed time since the earthquake (hour)

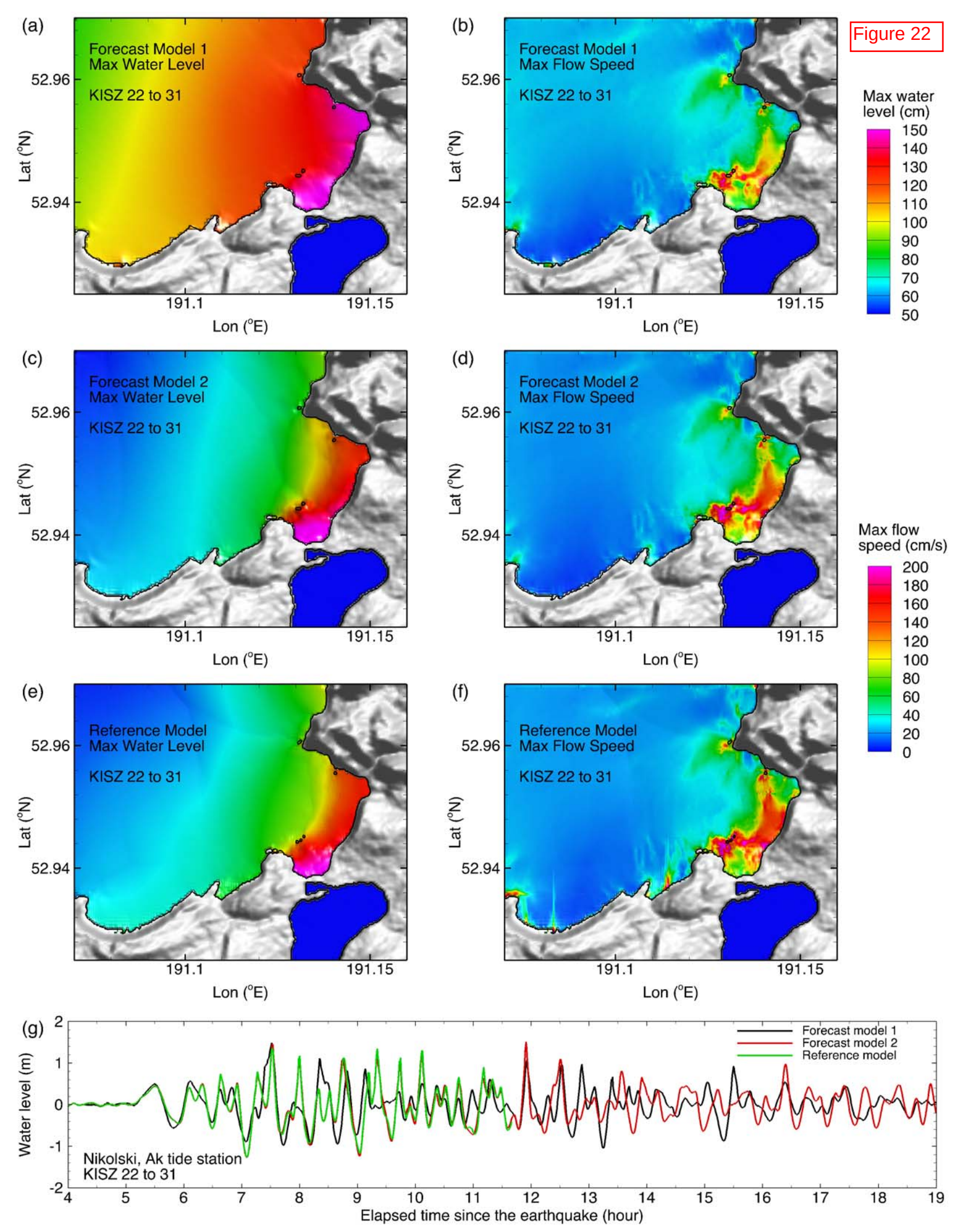
Figure 22
(a)
Forecast Model 1
Max Water Level
KISZ 22 to 31
(b)
Forecast Model 1
Max Flow Speed
KISZ 22 to 31
Max water level (cm)
150
140
130
120
110
100
90
80
70
60
50
(c)
Forecast Model 2
Max Water Level
KISZ 22 to 31
(d)
Forecast Model 2
Max Flow Speed
KISZ 22 to 31
Max flow speed (cm/s)
200
180
160
140
120
100
80
60
40
20
0
(e)
Reference Model
Max Water Level
KISZ 22 to 31
(f)
Reference Model
Max Flow Speed
KISZ 22 to 31
52.96
52.94
Lat (°N)
191.1
191.15
Lon (°E)
(g)
Water level (m)
2
1
0
-1
-2
Nikolski, Ak tide station
KISZ 22 to 31
Forecast model 1
Forecast model 2
Reference model
4
5
6
7
8
9
10
11
12
13
14
15
16
17
18
19
Elapsed time since the earthquake (hour)

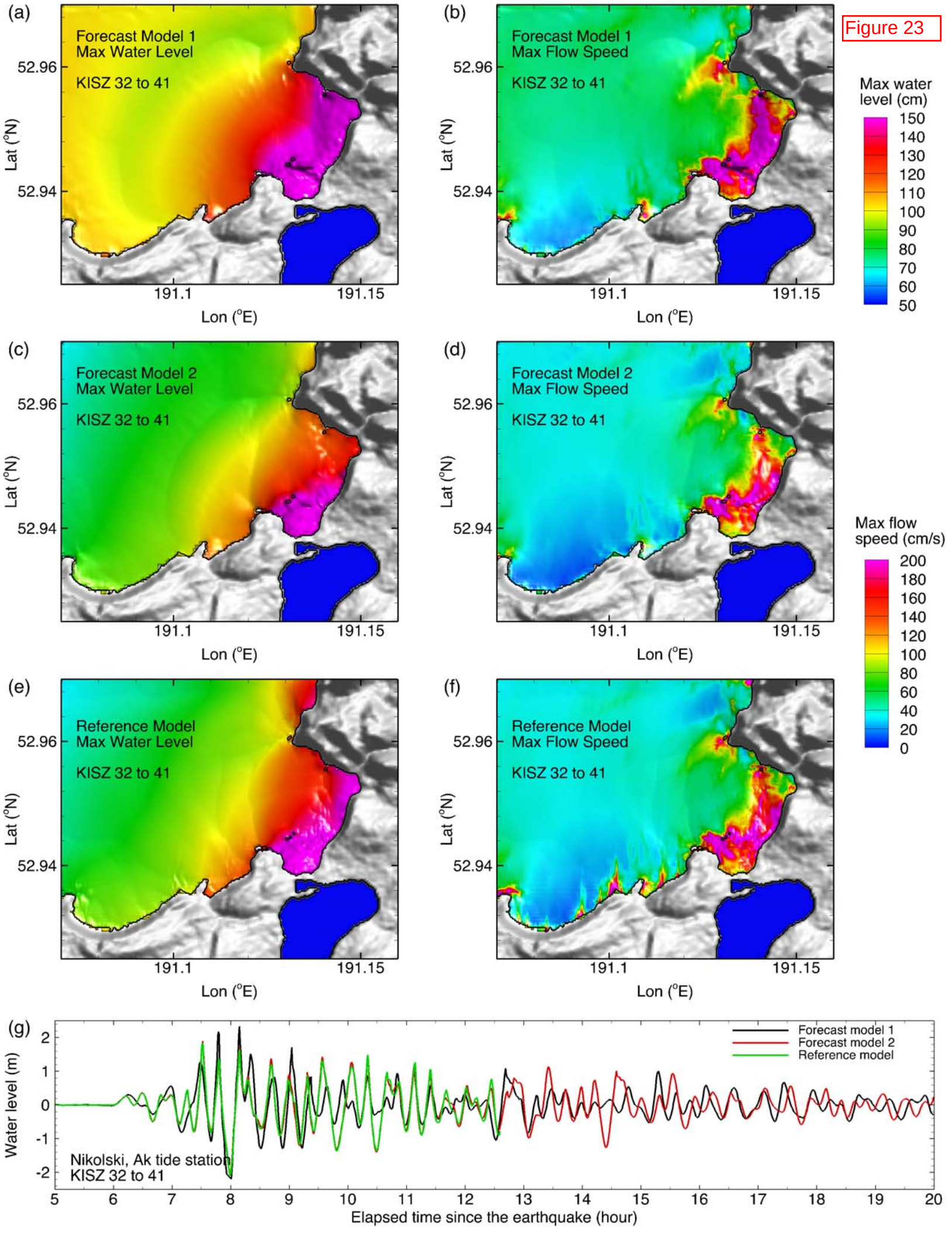
Figure 23
(a)
Forecast Model 1
Max Water Level
KISZ 32 to 41
(b)
Forecast Model 1
Max Flow Speed
KISZ 32 to 41
Max water level (cm)
150
140
130
120
110
100
90
80
70
60
50
(c)
Forecast Model 2
Max Water Level
KISZ 32 to 41
(d)
Forecast Model 2
Max Flow Speed
KISZ 32 to 41
Max flow speed (cm/s)
200
180
160
140
120
100
80
60
40
20
0
(e)
Reference Model
Max Water Level
KISZ 32 to 41
(f)
Reference Model
Max Flow Speed
KISZ 32 to 41
52.96
52.94
Lat (°N)
191.1
191.15
Lon (°E)
(g)
Water level (m)
2
1
0
-1
-2
Nikolski, Ak tide station
KISZ 32 to 41
Forecast model 1
Forecast model 2
Reference model
5
6
7
8
9
10
11
12
13
14
15
16
17
18
19
20
Elapsed time since the earthquake (hour)

Figure 24

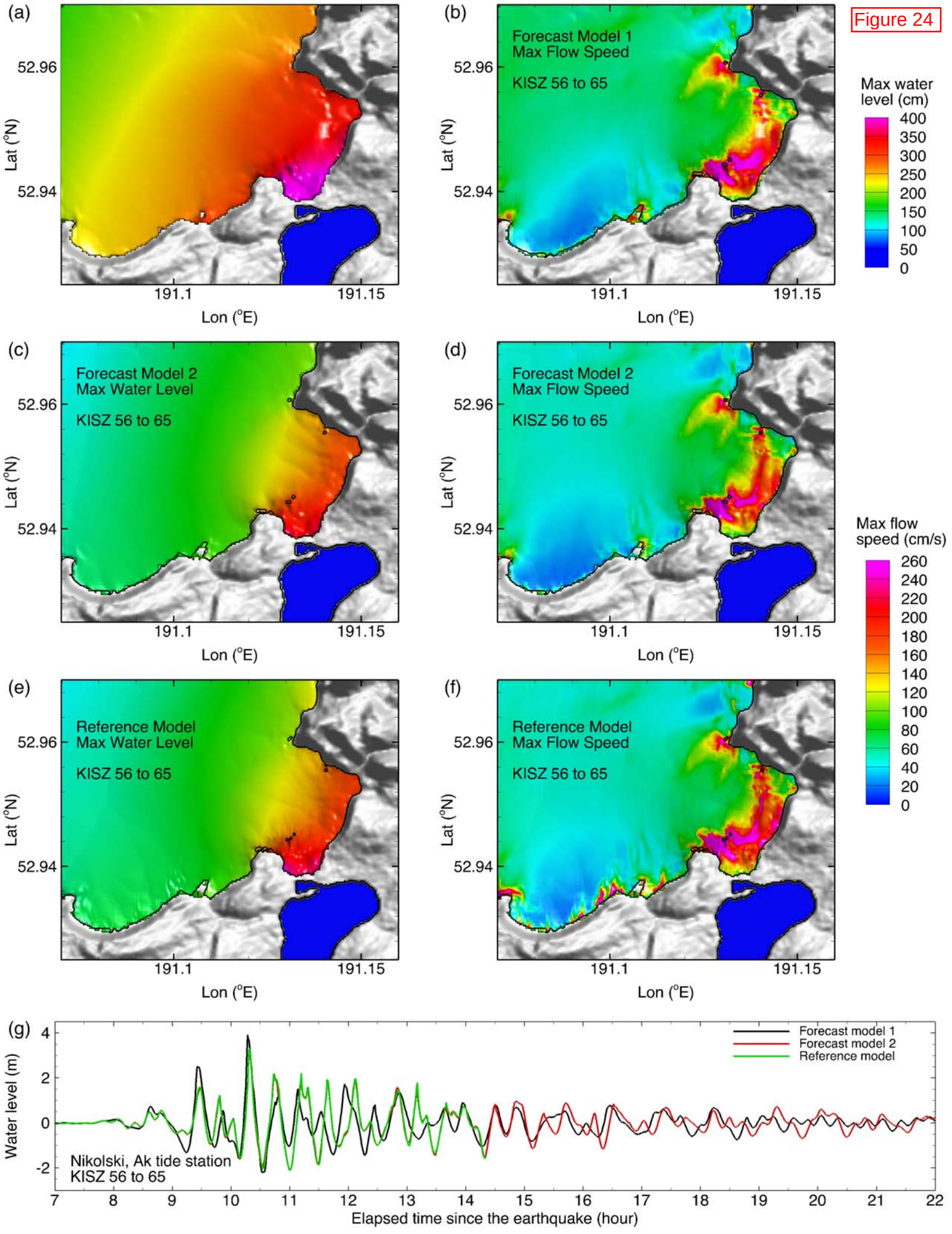
(a)
(b)
Forecast Model 1
Max Flow Speed
KISZ 56 to 65
Max water level (cm)
400
350
300
250
200
150
100
50
0
(c)
Forecast Model 2
Max Water Level
KISZ 56 to 65
(d)
Forecast Model 2
Max Flow Speed
KISZ 56 to 65
Max flow speed (cm/s)
260
240
220
200
180
160
140
120
100
80
60
40
20
0
(e)
Reference Model
Max Water Level
KISZ 56 to 65
(f)
Reference Model
Max Flow Speed
KISZ 56 to 65
52.96
52.94
Lat (°N)
191.1
191.15
Lon (°E)
(g)
Water level (m)
4
2
0
-2
Nikolski, Ak tide station
KISZ 56 to 65
Forecast model 1
Forecast model 2
Reference model
7
8
9
10
11
12
13
14
15
16
17
18
19
20
21
22
Elapsed time since the earthquake (hour)

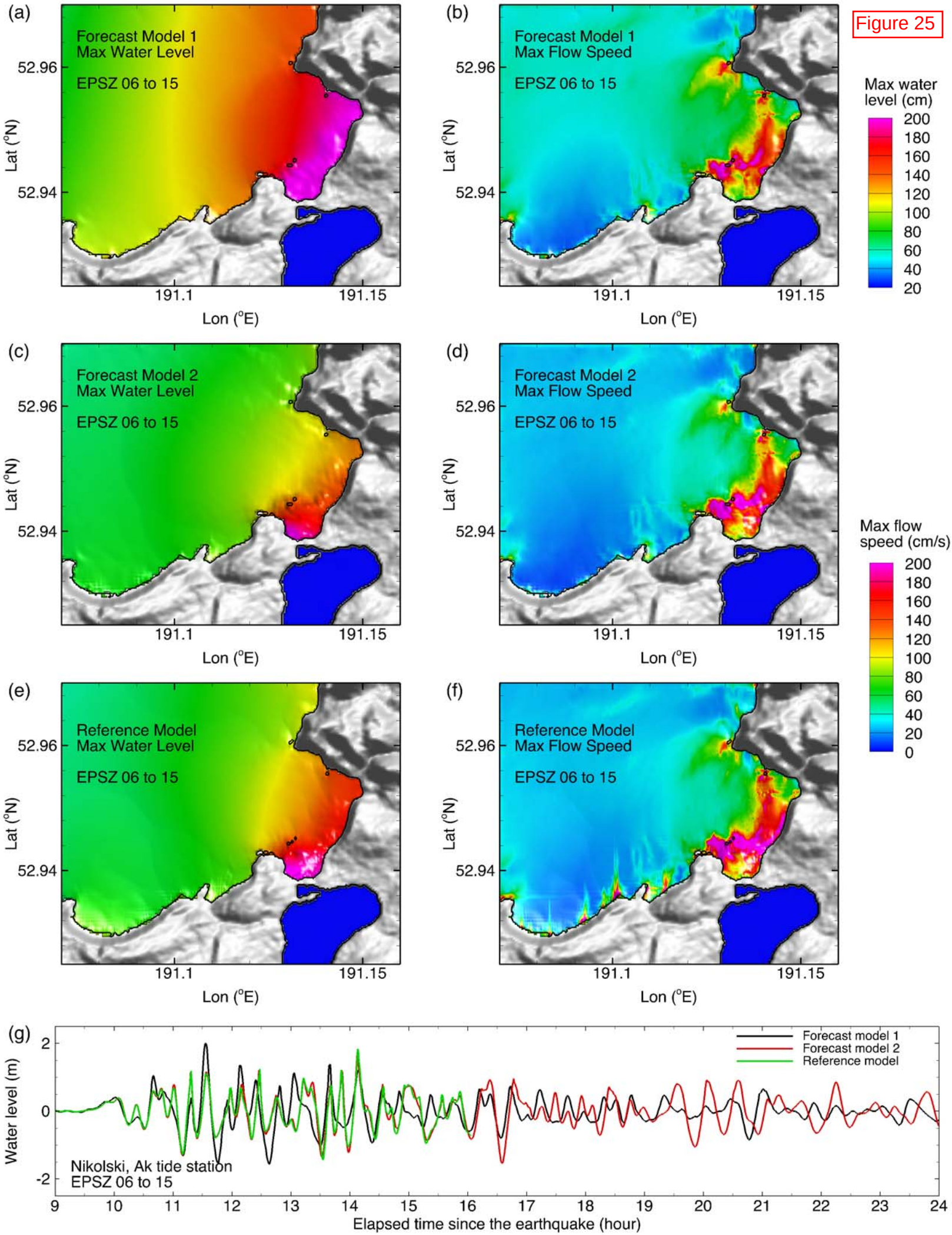
Figure 25
(a)
Forecast Model 1
Max Water Level
EPSZ 06 to 15
(b)
Forecast Model 1
Max Flow Speed
EPSZ 06 to 15
Max water level (cm)
200
180
160
140
120
100
80
60
40
20
(c)
Forecast Model 2
Max Water Level
EPSZ 06 to 15
(d)
Forecast Model 2
Max Flow Speed
EPSZ 06 to 15
Max flow speed (cm/s)
200
180
160
140
120
100
80
60
40
20
0
(e)
Reference Model
Max Water Level
EPSZ 06 to 15
(f)
Reference Model
Max Flow Speed
EPSZ 06 to 15
52.96
52.94
Lat (°N)
191.1
191.15
Lon (°E)
(g)
Forecast model 1
Forecast model 2
Reference model
Water level (m)
2
0
-2
Nikolski, Ak tide station
EPSZ 06 to 15
9
10
11
12
13
14
15
16
17
18
19
20
21
22
23
24
Elapsed time since the earthquake (hour)

Figure 26

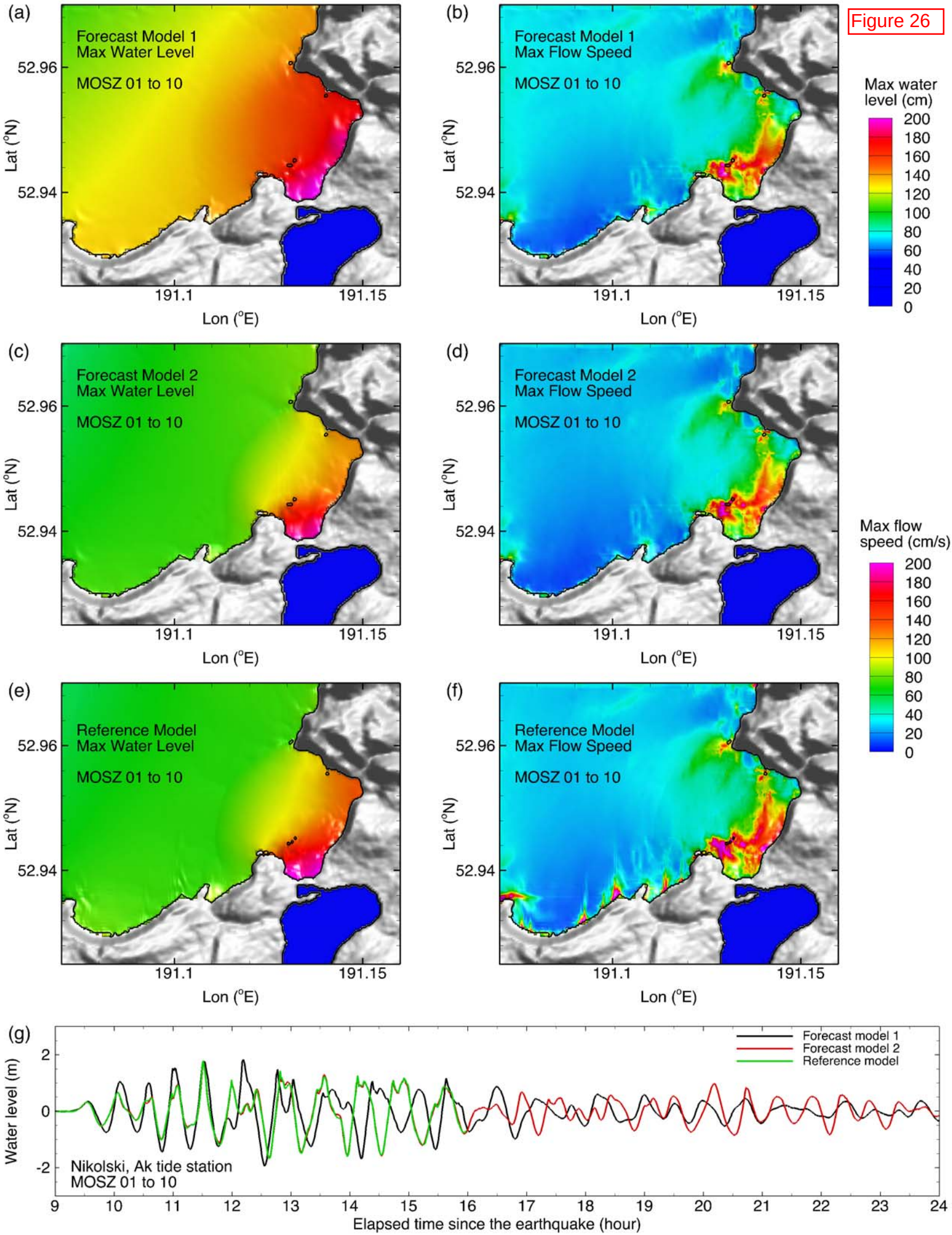
(a)
Forecast Model 1
Max Water Level
MOSZ 01 to 10
(b)
Forecast Model 1
Max Flow Speed
MOSZ 01 to 10
Max water level (cm)
200
180
160
140
120
100
80
60
40
20
0
(c)
Forecast Model 2
Max Water Level
MOSZ 01 to 10
(d)
Forecast Model 2
Max Flow Speed
MOSZ 01 to 10
Max flow speed (cm/s)
200
180
160
140
120
100
80
60
40
20
0
(e)
Reference Model
Max Water Level
MOSZ 01 to 10
(f)
Reference Model
Max Flow Speed
MOSZ 01 to 10
52.96
52.94
Lat (°N)
191.1
191.15
Lon (°E)
(g)
Water level (m)
2
0
-2
Nikolski, Ak tide station
MOSZ 01 to 10
Forecast model 1
Forecast model 2
Reference model
9
10
11
12
13
14
15
16
17
18
19
20
21
22
23
24
Elapsed time since the earthquake (hour)

Figure 27

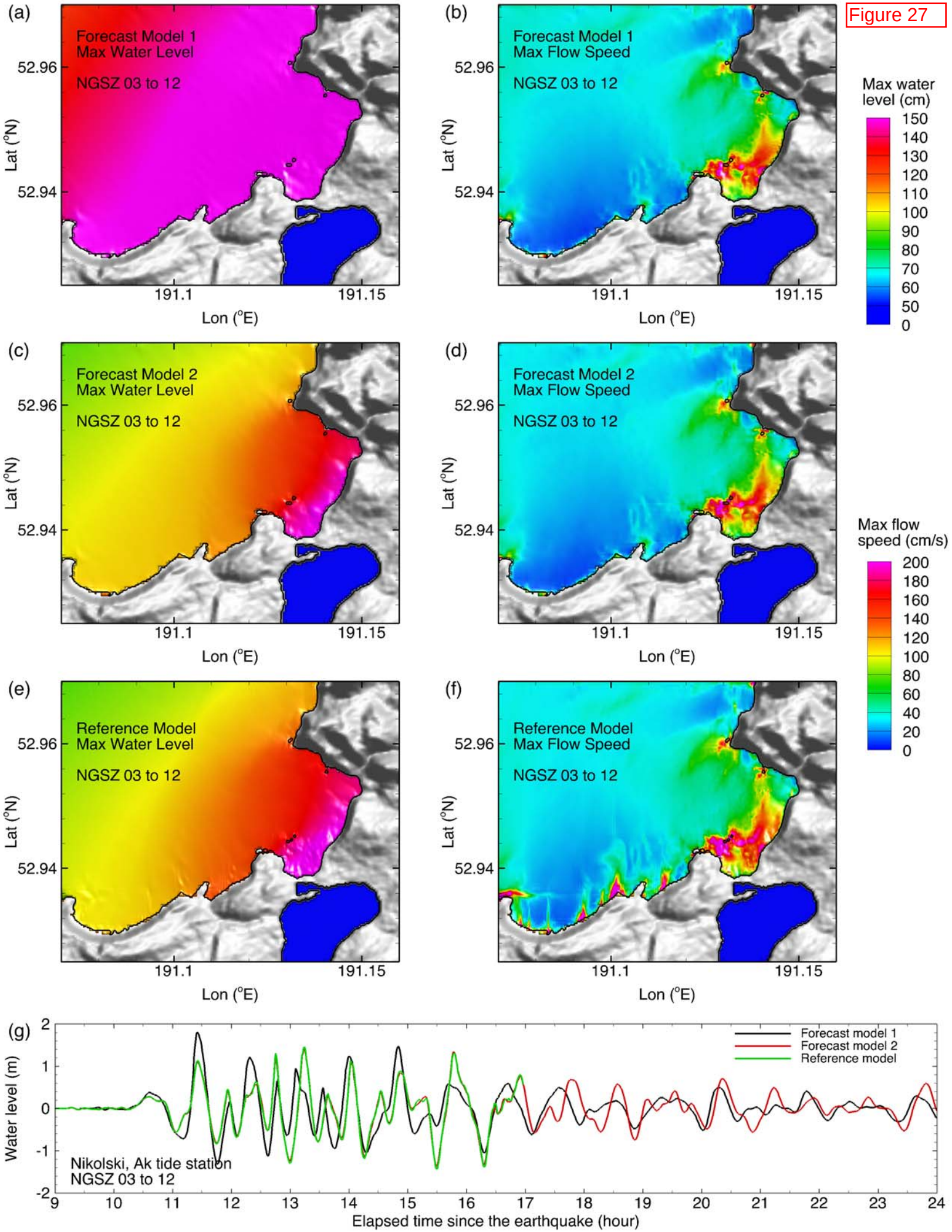
(a)
Forecast Model 1
Max Water Level
NGSZ 03 to 12
(b)
Forecast Model 1
Max Flow Speed
NGSZ 03 to 12
Max water level (cm)
150
140
130
120
110
100
90
80
70
60
50
0
(c)
Forecast Model 2
Max Water Level
NGSZ 03 to 12
(d)
Forecast Model 2
Max Flow Speed
NGSZ 03 to 12
Max flow speed (cm/s)
200
180
160
140
120
100
80
60
40
20
0
(e)
Reference Model
Max Water Level
NGSZ 03 to 12
(f)
Reference Model
Max Flow Speed
NGSZ 03 to 12
52.96
52.94
Lat (°N)
191.1
191.15
Lon (°E)
(g)
Water level (m)
2
1
0
-1
-2
Nikolski, Ak tide station
NGSZ 03 to 12
Forecast model 1
Forecast model 2
Reference model
9
10
11
12
13
14
15
16
17
18
19
20
21
22
23
24
Elapsed time since the earthquake (hour)

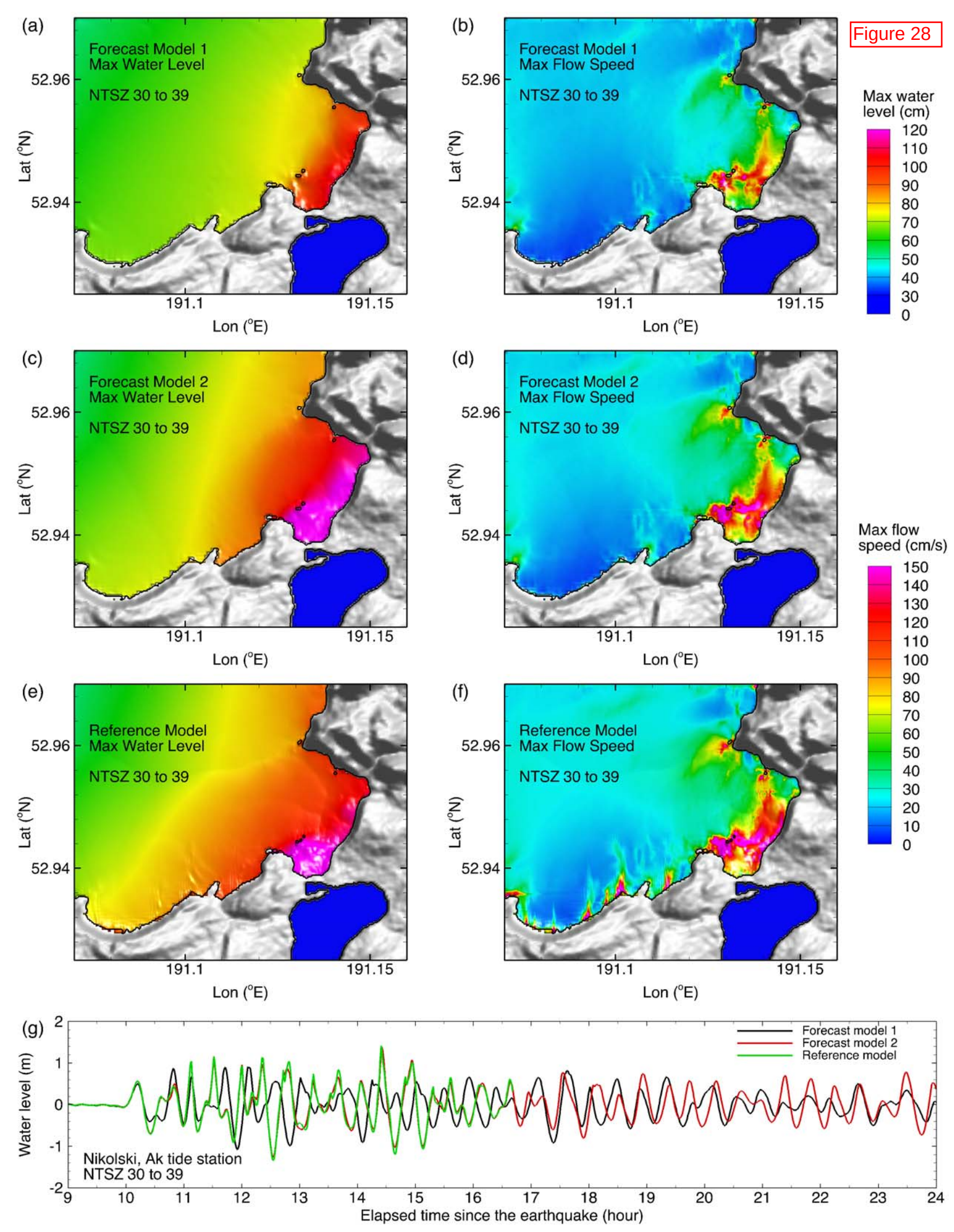
Figure 28
(a)
Forecast Model 1
Max Water Level
NTSZ 30 to 39
(b)
Forecast Model 1
Max Flow Speed
NTSZ 30 to 39
Max water level (cm)
120
110
100
90
80
70
60
50
40
30
0
(c)
Forecast Model 2
Max Water Level
NTSZ 30 to 39
(d)
Forecast Model 2
Max Flow Speed
NTSZ 30 to 39
Max flow speed (cm/s)
150
140
130
120
110
100
90
80
70
60
50
40
30
20
10
0
(e)
Reference Model
Max Water Level
NTSZ 30 to 39
(f)
Reference Model
Max Flow Speed
NTSZ 30 to 39
52.96
52.94
Lat (°N)
191.1
191.15
Lon (°E)
(g)
Water level (m)
2
1
0
-1
-2
Nikolski, Ak tide station
NTSZ 30 to 39
Forecast model 1
Forecast model 2
Reference model
9
10
11
12
13
14
15
16
17
18
19
20
21
22
23
24
Elapsed time since the earthquake (hour)

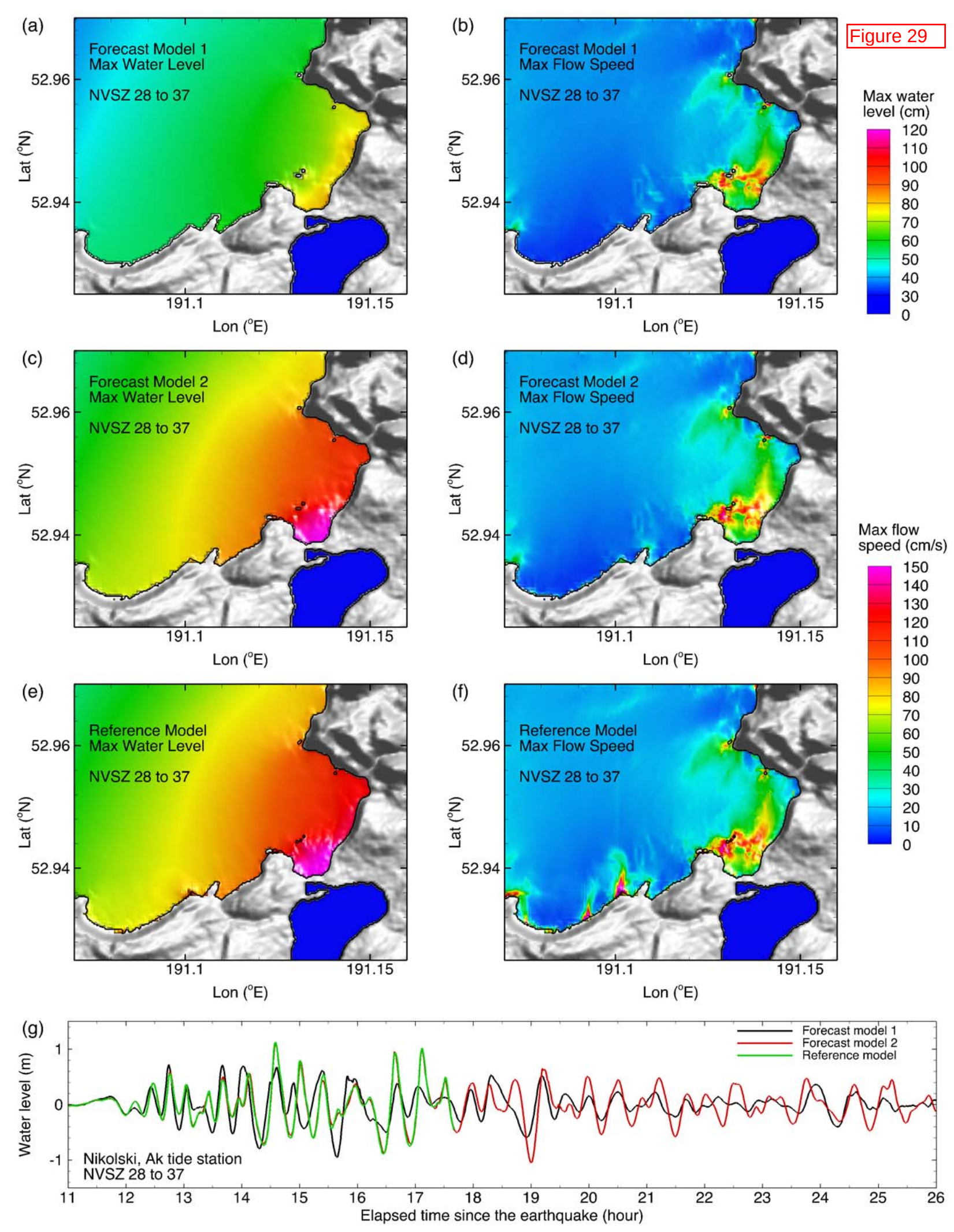
Figure 29
(a)
Forecast Model 1
Max Water Level
NVSZ 28 to 37
(b)
Forecast Model 1
Max Flow Speed
NVSZ 28 to 37
Max water level (cm)
120
110
100
90
80
70
60
50
40
30
0
(c)
Forecast Model 2
Max Water Level
NVSZ 28 to 37
(d)
Forecast Model 2
Max Flow Speed
NVSZ 28 to 37
Max flow speed (cm/s)
150
140
130
120
110
100
90
80
70
60
50
40
30
20
10
0
(e)
Reference Model
Max Water Level
NVSZ 28 to 37
(f)
Reference Model
Max Flow Speed
NVSZ 28 to 37
52.96
52.94
Lat (°N)
191.1
191.15
Lon (°E)
(g)
Forecast model 1
Forecast model 2
Reference model
Water level (m)
1
0
-1
Nikolski, Ak tide station
NVSZ 28 to 37
11
12
13
14
15
16
17
18
19
20
21
22
23
24
25
26
Elapsed time since the earthquake (hour)

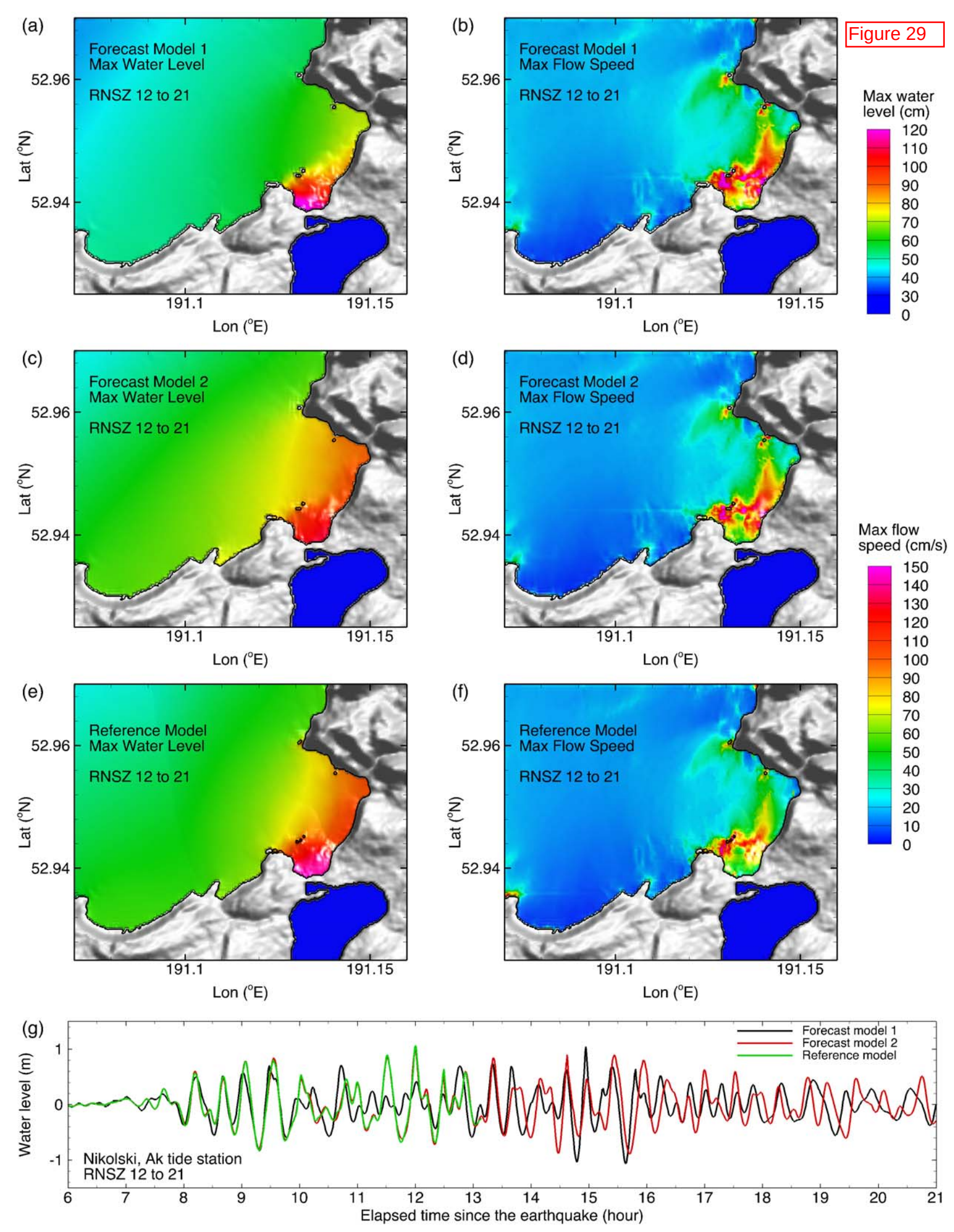
Figure 29
(a)
Forecast Model 1
Max Water Level
RNSZ 12 to 21
(b)
Forecast Model 1
Max Flow Speed
RNSZ 12 to 21
(c)
Forecast Model 2
Max Water Level
RNSZ 12 to 21
(d)
Forecast Model 2
Max Flow Speed
RNSZ 12 to 21
(e)
Reference Model
Max Water Level
RNSZ 12 to 21
(f)
Reference Model
Max Flow Speed
RNSZ 12 to 21
Lat (°N)
52.96
52.94
Lon (°E)
191.1
191.15
Max water level (cm)
120
110
100
90
80
70
60
50
40
30
0
Max flow speed (cm/s)
150
140
130
120
110
100
90
80
70
60
50
40
30
20
10
0
(g)
Water level (m)
1
0
-1
Nikolski, Ak tide station
RNSZ 12 to 21
Forecast model 1
Forecast model 2
Reference model
6
7
8
9
10
11
12
13
14
15
16
17
18
19
20
21
Elapsed time since the earthquake (hour)

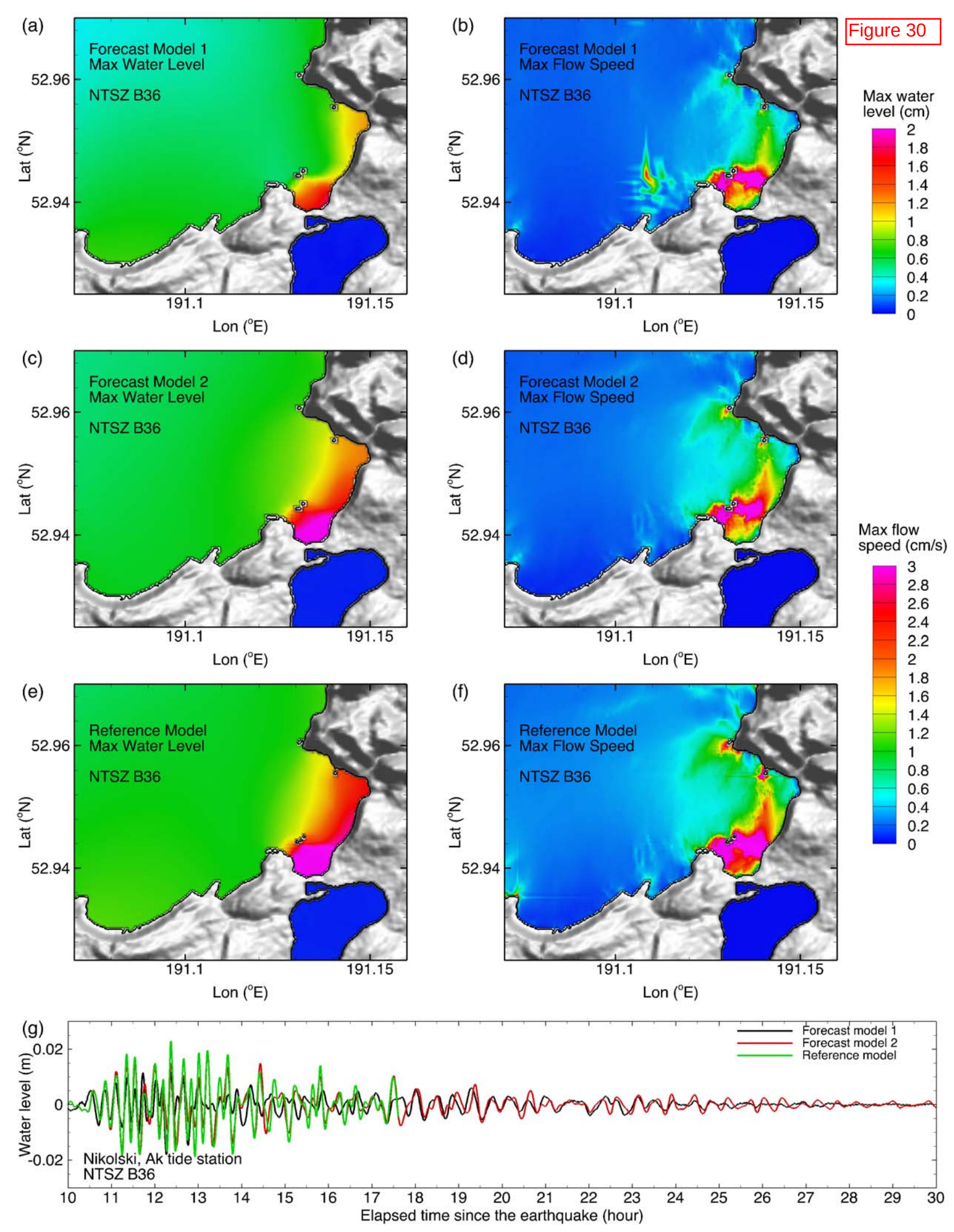
Figure 30
(a)
Forecast Model 1
Max Water Level
NTSZ B36
(b)
Forecast Model 1
Max Flow Speed
NTSZ B36
Max water level (cm)
2
1.8
1.6
1.4
1.2
1
0.8
0.6
0.4
0.2
0
(c)
Forecast Model 2
Max Water Level
NTSZ B36
(d)
Forecast Model 2
Max Flow Speed
NTSZ B36
Max flow speed (cm/s)
3
2.8
2.6
2.4
2.2
2
1.8
1.6
1.4
1.2
1
0.8
0.6
0.4
0.2
0
(e)
Reference Model
Max Water Level
NTSZ B36
(f)
Reference Model
Max Flow Speed
NTSZ B36
52.96
52.94
Lat (°N)
191.1
191.15
Lon (°E)
(g)
Water level (m)
0.02
0
-0.02
Nikolski, Ak tide station
NTSZ B36
Forecast model 1
Forecast model 2
Reference model
10
11
12
13
14
15
16
17
18
19
20
21
22
23
24
25
26
27
28
29
30
Elapsed time since the earthquake (hour)